

Helicity-Dependent Showers and Matching with VINCIA

A. J. Larkoski¹, J.J. Lopez-Villarejo^{2,3}, and P. Skands²

¹: Center for Theoretical Physics, Massachusetts Institute of Technology, Cambridge, MA 02139 U.S.A.

²: Theoretical Physics, CERN CH-1211, Geneva 23, Switzerland

³: Univ. Autonoma de Madrid and IFT-UAM/CSIC, Madrid 28049, Spain

Abstract — We present an antenna-shower formalism that includes helicity dependence for massless partons. The formalism applies to both traditional (global) showers and to sector-based variants. We combine the shower with VINCIA’s multiplicative approach to matrix-element matching, generalized to operate on each helicity configuration separately. The result is a substantial gain in computational speed for high parton multiplicities. We present an implementation of both sector and global showers, with min/max variations, and helicity-dependent tree-level matching applied through $n \leq 4$ for $V/H \rightarrow q\bar{q} + n$ partons and through $n \leq 5$ for $H \rightarrow n$ gluons.

1 Introduction

Multi-leg amplitudes and their combination with parton-shower resummations, called ME/PS matching, are among the most active topics in current high-energy phenomenology (see [1] for a review). What ME/PS matching provides is a calculation that smoothly interpolates between fixed-order QCD (and QED) amplitudes in the high- p_{\perp} region and infinite-order logarithmic approximations in the low- p_{\perp} one. Importantly, the output of such calculations is in the form of fully hadronized “events”, which can be subjected to direct and detailed experimental comparison.

However, current state-of-the-art multileg ME/PS methods, such as CKKW-L [2,3], MLM [4], and MENLOPS [5], are rather computationally intensive, so that the most complex calculations can only be carried out on large clusters. The increase in computational time with the number of legs is partly due to the amplitudes becoming more complicated at each order, but more importantly these methods (which we refer to collectively as “slicing” methods [6]) algorithmically treat each multi-leg matching step as completely unrelated to all the others: a separate phase-space integration, event-generation, and event unweighting step is needed for each multiplicity. As shown in [7], much faster algorithms can be constructed by “nesting” the successive matching steps within each other, starting from the Born level and using an overestimating (“trial”) parton shower as the only additional phase-space generator. The matrix-element amplitudes can then be imprinted on the final answer by a simple Monte-Carlo veto step. This approach, which we refer to as the “multiplicative” method, was first developed for one additional leg in [8] and was generalized to multiple legs in [9].

In this paper, we develop an additional refinement of the multiplicative method, which further increases the algorithmic speed that can be achieved when matching to large parton multiplicities. As a beneficial side effect, the intrinsic precision of the underlying parton-shower formalism is increased

as well. The main point is to replace the ordinary (helicity-summed) shower radiation functions with helicity-dependent ones, such as those given in [10]. That is, we shall treat (massless) quarks and gluons with negative and positive helicities as effectively being different particles. The resulting shower generates a LL approximation to each individual multi-leg helicity amplitude (squared) separately, and the resulting evolution can therefore be matched to one single such amplitude at a time. Thus, instead of taking sums and averages at each order, we are now effectively sampling helicity space by Monte Carlo, saving substantial time when matching to several successive legs.

Note that, up to the matched orders, interference effects between amplitudes with different internal helicity structures are still fully taken into account, since the last matched helicity amplitude does contain a sum over all contributing internal-line helicities. At subsequent orders, however, the helicity-dependent shower does not generate the equivalent of a full spin-density matrix treatment (see e.g. [11]). Nor are any explicit azimuth-dependent correlations among successive emissions manifest in the helicity basis as would be the case with linearly polarized Altarelli-Parisi kernels [12]. The final precision is nevertheless still improved, since unphysical helicity assignments are not allowed to contribute.

In section 2, we generalize the VINCIA shower and matching formalism [13] to include helicity dependence. In section 3, we derive explicit helicity-dependent QCD antenna functions, considering both sector and global antenna types. Finally, in section 4 we present a set of comparisons to matrix elements, speed benchmarks, and validations on selected LEP distributions, and in section 5 we summarize and provide a brief outlook.

2 The Shower and Matching Algorithm

The helicity of a particle is the projection of the spin of the particle onto its momentum. For massless particles, helicity is Lorentz invariant and takes the values $\pm s$ for particles with total spin s . Typically, in computing matrix elements, one sums over helicities of the incoming and outgoing particles because they are not directly observed. However, beginning with observations by Parke and Taylor [14] in the 1980s, it was discovered that individual helicity amplitudes are significantly simpler in form than are helicity-summed matrix elements. In addition, chirality or handedness is important in processes mediated by the weak interaction. Thus, we expect that a Monte Carlo parton shower based on the helicity structure of QCD, rather than summed over helicities, is both faster when matching to matrix elements as well as more accurate, especially in weak decays.

In this section, we discuss the modifications to the VINCIA shower and matching algorithms required to take helicity into account. The antenna functions themselves will be the topic of section 3.

2.1 Helicity-Dependent Showering

The helicity-dependent shower algorithm follows the unpolarized one quite closely [13], with differences entering only in a few very specific places, as follows.

If VINCIA is asked to shower an event that contains unpolarized partons, e.g. an unpolarized $Z \rightarrow q\bar{q}$ event, it first hands the event to a *polarizer* function which searches the VINCIA library for helicity-dependent matrix elements corresponding to the given process (see section 2.2 below for a full list). If this search is successful, helicities for the final-state partons are assigned based on their relative matrix-element weights. In the example of on-shell $Z \rightarrow d\bar{d}$ ($Z \rightarrow u\bar{u}$) decay, a phase-space-dependent average of 97% (83%) of the events will end up as $q_L\bar{q}_R$, with the other being $q_R\bar{q}_L$. For off-shell Z bosons, the full $e^+e^- \rightarrow \gamma^*/Z \rightarrow q\bar{q}$ matrix elements would be used instead.

Trial branchings are generated as in the unpolarized shower, according to the unpolarized trial functions. The unpolarized trial functions are essentially an overestimating eikonal term, see [9], with additional collinear-singular terms for sector showers [7]. After the selection of branching invariants, the probability that the branching will be accepted at all, summed over all possible post-branching helicities, is computed:

$$P_{\text{accept}} = \frac{a_{\text{phys}}}{a_{\text{trial}}} = \frac{\sum_{h_i, h_j, h_k} a(h_A, h_B \rightarrow h_i, h_j, h_k)}{a_{\text{trial}}}, \quad (1)$$

with $h_{A,B}$ the (fixed) helicities of the parent partons, $h_{i,j,k}$ the helicities of the daughter ones, and $a(h_A, h_B \rightarrow h_i, h_j, h_k)$ a helicity-dependent antenna function, the precise forms of which will be discussed in section 3. This accept probability is not exactly identical to the unpolarized one, since the helicities of the parent partons A and B are not averaged over. Note also that, for sector showers, the trial function appearing in the denominator should be the full one containing both the soft-eikonal and the additional collinear-singular trial terms.

Helicities for the three daughter partons are then assigned according to the relative probabilities

$$P(h_A, h_B \rightarrow h_i, h_j, h_k) = \frac{a(h_A, h_B \rightarrow h_i, h_j, h_k)}{\sum_{h_i, h_j, h_k} a(h_A, h_B \rightarrow h_i, h_j, h_k)}. \quad (2)$$

Note that it is important that the denominator here be exactly the same as the numerator in eq. (1).

All other aspects of the showering remain unmodified (for matching, see below). For completeness, we also note that, when helicity dependence is switched off, the unpolarized antenna functions are obtained as direct helicity sums over the helicity-dependent ones, averaging over the parent helicities. The treatments with and without helicity dependence are thus intimately related and it is straightforward to go from one to the other.

For one showering step, there should therefore also be little difference between the helicity-dependent and unpolarized treatments, up to differences caused by the helicity-dependent finite terms not being equal to their averages. However, the chosen helicities at one step then become the input helicities for the next step. This excludes some unphysical configurations from the effective helicity average/sum in the next step, yielding an improvement in accuracy over the unpolarized case.

2.2 Matching to Matrix Elements

The procedure for matching helicity matrix elements to the helicity-dependent parton shower in VIN-CIA is similar for matching to spin-summed matrix elements [9]. At each step in the shower, the parton shower provides an estimate for the ratio

$$P_n = \frac{|\mathcal{M}_n|^2}{|\mathcal{M}_{n-1}|^2}, \quad (3)$$

where $|\mathcal{M}_n|^2$ is the matrix element after n additional quark or gluon emissions from the Born-level matrix element. To match the parton shower to the exact matrix element at this stage, the emission of the n th parton is accepted with the probability

$$P_{\text{accept}}^n = \frac{a^{\text{Phys}}}{a^{\text{Trial}}} P_{\text{ME}}. \quad (4)$$

a^{Phys} is the antenna for the current branching and a^{Trial} is an overestimate antenna that is strictly larger than a^{Phys} . The matching factor P_{ME} is

$$P_{\text{ME}} = \frac{|\mathcal{M}_n|^2}{|\mathcal{M}_n|_{\text{shower}}^2}, \quad (5)$$

where $|\mathcal{M}_n|_{\text{shower}}^2$ is the approximation to the matrix element provided by the parton shower:

$$|\mathcal{M}_n|_{\text{shower}}^2 = \sum_i a_i |\mathcal{M}_{n-1 i}|^2, \quad (6)$$

with i running over the possible clusterings and helicities and a_i the corresponding antenna for the i th configuration. Note that the form of this approximation depends on the formulation of the shower (global vs. sector); see [7] for details on the differences between global and sector matching.

The ratio P_n in a helicity-dependent shower has especially nice and general properties. For decays of colorless resonances to massless quarks, P_n is independent of the CP structure of the resonance for helicity matrix elements. This allows the use of, for example, matrix elements for Z decay to massless quarks for use in matching processes which include W bosons or photons. Only the total spin of the resonance is relevant for matching to helicity matrix elements.

The proof of this is straightforward. Consider the ratio of amplitudes

$$\rho \equiv \frac{\mathcal{M}_n}{\mathcal{M}_{n-1}}. \quad (7)$$

This can be written generically as

$$\rho = \frac{\mathcal{M}_n}{\mathcal{M}_{n-1}} = \frac{\bar{u}(q_f) \mathcal{O}_g^n \not{J} (a - b\gamma_5) \mathcal{O}_g^n u(\bar{q}_f)}{\bar{u}(q_i) \mathcal{O}_g^{n-1} \not{J} (a - b\gamma_5) \mathcal{O}_g^{n-1} u(\bar{q}_i)}, \quad (8)$$

where q_i, q_f (\bar{q}_i, \bar{q}_f) are the (anti)quark before and after additional radiation, respectively, \not{J} is the current carried by the resonance, $(a - b\gamma_5)$ parametrizes the CP structure of the current, and \mathcal{O}_g^n is an unspecified operator which produces additional QCD radiation up to $\mathcal{O}(g_s^n)$. Irrespective of the form of the current \not{J} , the radiation operators \mathcal{O}_g^n and \mathcal{O}_g^{n-1} contain an even number of gamma matrices: one for each quark-gluon vertex and one for each quark propagator. Then, it is true that

$$[\mathcal{O}_g^n, \gamma_5] = [\mathcal{O}_g^{n-1}, \gamma_5] = 0, \quad (9)$$

which allows us to freely interchange the position of $(a - b\gamma_5)$ and \mathcal{O}_g . We then have

$$\rho = \frac{\mathcal{M}_n}{\mathcal{M}_{n-1}} = \frac{\bar{u}(q_f) \mathcal{O}_g^n \not{J} \mathcal{O}_g^n (a - b\gamma_5) u(\bar{q}_f)}{\bar{u}(q_i) \mathcal{O}_g^{n-1} \not{J} \mathcal{O}_g^{n-1} (a - b\gamma_5) u(\bar{q}_i)}. \quad (10)$$

Helicity spinors are eigenvectors of γ_5 with eigenvalue equal to their helicity. The helicity of massless quarks is preserved in QCD; that is,

$$\gamma_5 u(\bar{q}) = h_{\bar{q}} u(\bar{q}) \quad \text{and} \quad h_{\bar{q}_i} = h_{\bar{q}_f}. \quad (11)$$

We then find that

$$\rho = \frac{\bar{u}(q_f) \mathcal{O}_g^n \not{J} \mathcal{O}_g^n u(\bar{q}_f) (a - bh_{\bar{q}})}{\bar{u}(q_i) \mathcal{O}_g^{n-1} \not{J} \mathcal{O}_g^{n-1} u(\bar{q}_i) (a - bh_{\bar{q}})} = \frac{\bar{u}(q_f) \mathcal{O}_g^n \not{J} \mathcal{O}_g^n u(\bar{q}_f)}{\bar{u}(q_i) \mathcal{O}_g^{n-1} \not{J} \mathcal{O}_g^{n-1} u(\bar{q}_i)}, \quad (12)$$

proving that P_n is independent of the CP structure of the resonance. Note that by crossing symmetry, this proof also holds for particles created in the final state from parton-parton scattering.

Based on the universality of P_n , the current VINCIA implementation includes matching to the helicity amplitudes listed in tab. 1, with V and S denoting a generic colorless spin-1 and spin-0 particle, respectively. The corresponding massless helicity amplitudes squared were obtained by modifying

Decaying Particle	Order Beyond Born				
	0	1	2	3	4
V, S	$q\bar{q}$	$q\bar{q}g$	$q\bar{q}gg, q\bar{q}q'\bar{q}'$	$q\bar{q}ggg, q\bar{q}q\bar{q}'g$	$q\bar{q}gggg, q\bar{q}q'\bar{q}'gg, q\bar{q}q'\bar{q}''q''$
S	gg	ggg	$gggg$	$ggggg$	-

Table 1: Matrix elements available in VINCIA for helicity-dependent matching corrections, with V (S) a generic colorless spin-1 (spin-0) boson with arbitrary couplings.

MADGRAPH v. 4.4.26 [18] to extract individual helicity configurations and are evaluated at runtime using the HELAS libraries [19]. For processes involving decaying massive vector bosons, the spin of the vector is summed over in computing the helicity matrix element. In addition, matching is done for on-shell particles and so the mass of the decaying resonance is artificially set to the center of mass energy Q . Note that the HELAS libraries are so far not included in the VINCIA package itself and must be downloaded separately. The default VINCIA `make` target will automatically attempt to download the MADGRAPH package and compile the HELAS library from there. Alternatively, the user has the option of providing a precompiled HELAS library.

2.3 Massive Partons

The helicity-dependent formalism presented in this paper is limited to massless partons. For massive partons, VINCIA reverts to the unpolarized massive framework presented in [20]. By default, this applies to charm and heavier quarks. User options are provided that allow the massive treatment to be applied also to s quarks, or to force c and/or b ones to be treated as massless. For completeness, we describe here what the code does when helicity-dependence is switched on (as it is by default) and one or more massive partons are present either in the Born-level event (e.g., via a $Z \rightarrow b\bar{b}$ decay) or are created during the shower evolution (e.g., via a $g \rightarrow b\bar{b}$ splitting).

If a massive parton is present already in the Born-level event, the entire event is treated as unpolarized. That is, all parton helicities are ignored, including those of massless partons. The massive shower algorithm described in [20] is applied, and hence mass corrections are included, even if helicity-dependence is not.

If no massive parton is present in the Born-level event, the helicity-dependent shower described in this paper is applied to the event, but trial splittings of gluons to massive quarks are still allowed. If such a branching is accepted, all helicities are then ignored *from that point onwards*, and the further event evolution proceeds according to the unpolarized algorithm [20], as above.

A subtlety arises concerning the matching to matrix elements. As described above, the helicity-dependent formalism allows us to use matrix elements for Z decay to represent any vector boson, and ones for H decay to represent any scalar. For spin-summed matrix elements, however, this universality breaks down. The user should therefore be aware that, while the full range of matched matrix elements are still available for Z and H^0 decays to unpolarized massive particles, the corresponding corrections for W and H^\pm decays to massive partons have so far not been implemented.

For future reference, we note that phase-space maps for antennae involving massive particles are available in [20] and a set of spin-dependent antenna functions were defined in [21].

	++	-+	+−	--
$g_+ \rightarrow gg$	$1/z(1-z)$	$(1-z)^3/z$	$z^3/(1-z)$	0
$g_+ \rightarrow q\bar{q}$	-	$(1-z)^2$	z^2	-
$q_+ \rightarrow qg$	$1/(1-z)$	-	$z^2/(1-z)$	-
$q_+ \rightarrow gq$	$1/z$	$(1-z)^2/z$	-	-

Table 2: Helicity-dependent Altarelli-Parisi splitting functions $P(z)$ for splittings $a \rightarrow bc$, with z defined as the energy fraction taken by parton b . The labels in the top row denote the helicities of the two final particles in the order they appear: (h_b, h_c) . The empty columns are forbidden by quark chiral symmetry. By the P and C invariance of QCD, the same expressions apply after exchanging $- \leftrightarrow +$ or $q \leftrightarrow \bar{q}$.

3 Helicity-Dependent Antenna Functions

Parton showers (including the dipole/antenna varieties) are governed by the properties of soft and collinear emissions in QCD. The soft and collinear limits of massless QCD matrix elements are the universal Altarelli-Parisi splitting functions [15] and take the schematic form

$$\lim_{s_{ij} \rightarrow 0} |\mathcal{M}(1, \dots, i, j, \dots, n)|^2 = \frac{1}{s_{ij}} g_s^2 \mathcal{C}_{ij} P_{i,j \leftarrow \hat{ij}}(z) |\mathcal{M}(1, \dots, \hat{ij}, \dots, n)|^2, \quad (13)$$

where \mathcal{C}_{ij} is the color factor, $g_s^2 = 4\pi\alpha_s$ is the QCD coupling and particles i and j are replaced by \hat{ij} in the matrix element on the right. $P_{i,j \leftarrow \hat{ij}}(z)$ is the splitting function representing the distribution of energy fraction z carried by particle i . The Altarelli-Parisi splitting functions for massless quarks and gluons of definite helicity were given in their original paper and are reproduced in tab. 2. Note that rows in tab. 2 sum to the familiar, unpolarized, Altarelli-Parisi splitting functions.

The VINCIA Monte Carlo is a dipole-antenna shower [13] based on nested $2 \rightarrow 3$ splitting processes. This splitting can be represented as $IK \rightarrow ijk$, for initial partons I, K and final partons i, j, k . As VINCIA works in the color-ordered limit of QCD, the initial and final partons are assumed to be in color order, as well. We will also assume that all partons are massless, unless otherwise specified. The phase space for emission is defined by the dimensionless variables y_{ij} and y_{jk} where

$$y_{ij} = \frac{2p_i \cdot p_j}{s}, \quad y_{jk} = \frac{2p_j \cdot p_k}{s}, \quad (14)$$

and $s \equiv (p_i + p_j + p_k)^2 = (p_I + p_K)^2$ is the invariant mass of the dipole antenna system. The phase space of the emission is defined by the triangle $y_{ij}, y_{jk} \geq 0, y_{ij} + y_{jk} \leq 1$.

The probability of emission is governed by the antenna function which is a function of all relevant momenta, quantum numbers and the formulation of the shower. For the splitting $IK \rightarrow ijk$, the antenna function can be expressed in the form

$$a_{j/IK}^{\text{type}(\text{order})}(p_i, p_j, p_k), \quad (15)$$

where type refers to global or sector antennae and order is the order in α_s to which the antennae are computed. When obvious from context, the superscripts will be omitted. In this paper, we will consider exclusively the lowest order antenna functions and so we can define the color- and coupling-stripped antenna

$$a_{j/IK}(p_i, p_j, p_k) = g_s^2 \mathcal{C}_{j/IK} \bar{a}_{j/IK}(p_i, p_j, p_k). \quad (16)$$

For simplicity, we will work with the color- and coupling-stripped antenna in the following. For massless partons, $\bar{a}_{j/IK}(p_i, p_j, p_k)$ is a function of the kinematic invariants y_{ij} and y_{jk} only.

The unpolarized global and sector antennae used in VINCIA were defined in [7, 9, 13]. We wish to extend the global and sector antennae to include full helicity dependence of all partons in the antenna. Our discussion will only include antennae in which all particles are massless. Antenna splitting functions including helicity dependence were defined in [10] as ratios of matrix elements, but here, we will present a general treatment of the form of the antennae. There are many constraints that must be imposed on the antennae to determine the singular terms; most importantly, the helicity-dependent antenna functions must appropriately reproduce the helicity-dependent Altarelli-Parisi splitting functions in the collinear limits. Note that this only constrains the singular terms of the antenna; the non-singular terms are unconstrained and can be interpreted as uncertainties in higher log-order terms. Also, when summed over final parton helicities, the antenna functions should reproduce the unpolarized antennae functions, up to terms that are non-singular. In the following subsections, we will discuss the construction of global and sector helicity-dependent antennae.

Before discussing the global and sector antennae, we will distinguish the definition and utility of helicity to define a massless particle's spin from other definitions in the literature or used in simulation code. The Les Houches Accords of 2001 [16] outlined a set of variables by which to define the properties of particles in Monte Carlo event simulations. The variable `SPINUP` was introduced to quantify the spin of a particle and is defined to be:

`double SPINUP(I) : cosine of the angle between the spin-vector of particle I and
the 3- momentum of the decaying particle, specified in the lab frame`

This definition of spin for particles in Monte Carlos is unfortunately complicated and not widely applicable. Its use has been mainly restricted to treating polarized τ decays. In this and future work, we propose using chirality as the basis for defining spin for massive or massless fermions. Chirality is Lorentz invariant, relevant in weak decays and reduces to helicity for massless fermions.

Also, polarized splitting functions [12] should be distinguished from helicity splitting functions. It is first an issue of semantics. Helicity is the handedness of circular polarization of a particle with respect to its momentum. For massless particles, this is Lorentz invariant, as mentioned earlier. Polarized splitting functions instead reference the linear polarization of a particle with respect to the plane of the splitting. They are thus not Lorentz invariant, even for massless particles. However, polarized splitting functions can be used to approximate the azimuthal correlations between subsequent emissions and the effect on the energy distribution of the shower. Helicity splitting functions do not have this property; however, the azimuthal correlations do of course reappear when the shower is matched to matrix elements.

3.1 Global Antennae

The forms of the global antennae are found by enforcing several requirements. Global antennae contain the full soft limit of emitted gluons but neighboring antennae share a collinear limit of gluons. To construct the helicity-dependent global antennae, then, every possible helicity configuration of neighboring antennae must reproduce the correct collinear limits. Also the helicity dependent antennae can become negative over a significant region of phase space. For the use of the antennae functions as probability distributions on phase space they must be positive on all of phase space.

For the unpolarized global antennae, it is a straightforward exercise to incorporate all constraints to determine the antennae. We present an example of this in appendix A.1. The construction of helicity-dependent global antennae is more subtle, but we employ the following requirements to simplify the analysis:

\times	$\frac{1}{y_{ij}y_{jk}}$	$\frac{1}{y_{ij}}$	$\frac{1}{y_{jk}}$	$\frac{y_{jk}}{y_{ij}}$	$\frac{y_{ij}}{y_{jk}}$	$\frac{y_{jk}^2}{y_{ij}}$	$\frac{y_{ij}^2}{y_{jk}}$	1	y_{ij}	y_{jk}
<i>q\bar{q} \rightarrow qq\bar{q}</i>										
++ \rightarrow +++	1	0	0	0	0	0	0	0	0	0
++ \rightarrow +-+	1	-2	-2	1	1	0	0	2	0	0
+- \rightarrow ++-	1	0	-2	0	1	0	0	0	0	0
+- \rightarrow +--	1	-2	0	1	0	0	0	0	0	0
<i>gg \rightarrow qgg</i>										
++ \rightarrow +++	1	0	$-\alpha + 1$	0	$2\alpha - 2$	0	0	0	0	0
++ \rightarrow +-+	1	-2	-3	1	3	0	-1	3	0	0
+- \rightarrow ++-	1	0	-3	0	3	0	-1	0	0	0
+- \rightarrow +--	1	-2	$-\alpha + 1$	1	$2\alpha - 2$	0	0	0	0	0
<i>gg \rightarrow ggg</i>										
++ \rightarrow +++	1	$-\alpha + 1$	$-\alpha + 1$	$2\alpha - 2$	$2\alpha - 2$	0	0	0	0	0
++ \rightarrow +-+	1	-3	-3	3	3	-1	-1	3	1	1
+- \rightarrow ++-	1	$-\alpha + 1$	-3	$2\alpha - 2$	3	0	-1	0	0	0
+- \rightarrow +--	1	-3	$-\alpha + 1$	3	$2\alpha - 2$	-1	0	0	0	0
<i>gg \rightarrow q\bar{q}'q'</i>										
++ \rightarrow ++-	0	0	0	0	0	0	$\frac{1}{2}$	0	0	0
++ \rightarrow +-+	0	0	$\frac{1}{2}$	0	-1	0	$\frac{1}{2}$	0	0	0
+- \rightarrow ++-	0	0	$\frac{1}{2}$	0	-1	0	$\frac{1}{2}$	0	0	0
+- \rightarrow +-+	0	0	0	0	0	0	$\frac{1}{2}$	0	0	0
<i>gg \rightarrow g\bar{q}q</i>										
++ \rightarrow ++-	0	0	0	0	0	0	$\frac{1}{2}$	0	0	0
++ \rightarrow +-+	0	0	$\frac{1}{2}$	0	-1	0	$\frac{1}{2}$	0	0	0
+- \rightarrow ++-	0	0	$\frac{1}{2}$	0	-1	0	$\frac{1}{2}$	0	0	0
+- \rightarrow +-+	0	0	0	0	0	0	$\frac{1}{2}$	0	0	0

Table 3: Table of coefficients for helicity-dependent global antenna functions. By the C and P invariance of QCD, the same expressions apply with $+ \leftrightarrow -$, $q \leftrightarrow \bar{q}$. All other antennae are zero. The parameter α determines the form of the spin-summed global antennae. The default choice in VINCIA is $\alpha = 0$ which corresponds to the Gehrmann-De Ridder, Gehrmann, and Glover (GGG) spin-summed antennae [17]. The finite terms are chosen so that the antennae are positive on all of final-state phase space.

1. Bose-Einstein symmetry. The antenna functions must be symmetric when gluons of the same helicity are exchanged.
2. C and P symmetry of QCD. The expressions for the antennae are unchanged with $+$ \leftrightarrow $-$, $q \leftrightarrow \bar{q}$.
3. Neighboring antennae sum to reproduce the full collinear limits.
4. The singular terms of the helicity-dependent global antennae must sum to reproduce the singular terms of the unpolarized global antennae.
5. Positivity of global antennae. Because the collinear limits of gluons are constructed from the sum of neighboring antennae, the antennae are not guaranteed to be positive even in the singular regions of phase space. The positivity requirement must be enforced in the singular as well as non-singular regions of phase space.

A careful accounting of these requirements produces helicity-dependent global antennae that depend on three arbitrary parameters. One of these parameters fixes the form of the spin-summed or unpolarized antennae, which we call α , while the other two are artifacts of the proliferation of helicity-dependent antennae. The latter two parameters can consistently be set to zero, which we choose to do in the following. The complete procedure, with fully general expressions, is described in appendix A.2. Here, we just give the forms of the single-parameter antenna functions implemented in VINCIA, which are defined in tab. 3.

To estimate shower uncertainties due to the ambiguous choice of non-singular terms, we define a set of MIN and MAX antenna functions which are smaller and larger, respectively, over all of phase space than the default antennae. For the MAX antennae, the finite terms of all helicity-dependent antennae are fixed to a large constant value; we choose to set the constant to be 5.0. This is large enough to guarantee that all antennae are positive on phase space. MIN antennae are more subtle because some helicity-dependent antennae cannot be decreased and remain positive on phase space. To assuage this, we choose constants to subtract from those helicity-dependent antennae which are large and positive enough to allow this. (Specifically, we subtract the minimum value on the $2 \rightarrow 3$ phase-space of the singular pieces of the given antenna.) This procedure guarantees that, when summed over helicities, the MIN antennae are smaller than the default antennae in VINCIA. We present the choice of MIN antennae in tab. 4.

3.2 Sector Antennae

The helicity-dependent sector antennae are defined by reproducing the appropriate Altarelli-Parisi splitting functions as the emitted particle becomes collinear with respect to either of the initial particles. This requirement uniquely fixes the singular components of all sector antennae but still allows for freedom of the choice of non-singular terms in the antennae. The non-singular terms can be chosen so that the sector antennae reproduce matrix elements for particular processes, for example, which was done in [10]. Positivity of the sector antenna functions is guaranteed in the singular regions because the antennae reproduce the universal Altarelli-Parisi functions. However, for some antennae, non-singular pieces must be added to keep the antennae positive in the non-singular regions of phase space.

Defining the antenna functions by a ratio of matrix elements is one prescription for choosing the non-singular terms that are necessary to enforce positivity of the antenna on all of phase space. Our prescription for the choice of non-singular terms for the sector antennae is to add only the minimal

\times	$\frac{1}{y_{ij}y_{jk}}$	$\frac{1}{y_{ij}}$	$\frac{1}{y_{jk}}$	$\frac{y_{jk}}{y_{ij}}$	$\frac{y_{ij}}{y_{jk}}$	$\frac{y_{jk}^2}{y_{ij}}$	$\frac{y_{ij}^2}{y_{jk}}$	1
$q\bar{q} \rightarrow qq\bar{q}$								
$++ \rightarrow +++$	1	0	0	0	0	0	0	-4
$++ \rightarrow +-+$	1	-2	-2	1	1	0	0	2
$qg \rightarrow qgg$								
$++ \rightarrow +++$	1	0	1	0	-2	0	0	-3
$++ \rightarrow +-+$	1	-2	-3	1	3	0	-1	3
$gg \rightarrow ggg$								
$++ \rightarrow +++$	1	1	1	-2	-2	0	0	-4
$++ \rightarrow +-+$	1	-3	-3	3	3	-1	-1	3.7

Table 4: Table of coefficients for MIN helicity-dependent global antenna functions. In this table, α has been set to 0 which is the default choice in VINCIA. Only those antennae with non-zero finite terms are shown.

terms necessary. For antennae whose singular terms are positive on all of phase space, we choose to set the non-singular terms to 0. For those antennae which require the addition of non-singular terms for positivity, we choose to add constants where possible and only include higher order terms in y_{ij} and y_{jk} if necessary for simplicity. An example of the construction of sector antennae from the collinear limits and positivity is given in appendix A.3 and the coefficients of the terms in the sector antennae are given in tab. 5.

To estimate shower uncertainties due to the ambiguous choice of non-singular terms, we define a set of MIN and MAX antenna functions, as in the global shower case. For simplicity, the finite terms for the sector MIN and MAX antennae are chosen to be the same as those in the global case.

In the VINCIA code, the sector antennae are derived from the global antennae. Note from tab. 3 and tab. 5 that much of the structure of the sector antennae is captured by the global antennae if $\alpha = 1$. To construct a sector antenna, the corresponding global antenna with the same helicity and flavor structure is evaluated with $\alpha = 1$ and the missing terms added to recover the full sector antenna. The precise relationship between the sector (\bar{a}^{sect}) and global (\bar{a}^{gl}) antennae for $\alpha = 1$ for gluon emission is:

$$\begin{aligned}
\bar{a}_{j/IK}^{\text{sect}}(y_{ij}, y_{jk}) = & \bar{a}_{j/IK}^{\text{gl}}(y_{ij}, y_{jk}) + \delta_{Ig} \delta_{h_K h_k} \left\{ \delta_{h_I h_i} \delta_{h_I h_j} \left(\frac{1 + y_{jk} + y_{jk}^2}{y_{ij}} \right) \right. \\
& + \left. \delta_{h_I h_j} \left(\frac{1}{y_{ij}(1 - y_{jk})} - \frac{1 + y_{jk} + y_{jk}^2}{y_{ij}} \right) \right\} \\
& + \delta_{Kg} \delta_{h_I h_i} \left\{ \delta_{h_I h_j} \delta_{h_K h_k} \left(\frac{1 + y_{ij} + y_{ij}^2}{y_{jk}} \right) \right. \\
& + \left. \delta_{h_K h_j} \left(\frac{1}{y_{jk}(1 - y_{ij})} - \frac{1 + y_{ij} + y_{ij}^2}{y_{jk}} \right) \right\}.
\end{aligned}$$

Here, δ_{Ig} is one if I is a gluon and zero otherwise and $\delta_{h_i h_j}$ is one if the helicity of particles i and j are the same and zero otherwise. For antennae with gluons splitting to quarks, the sector antennae are twice the global antennae.

\times	$\frac{1}{y_{ij}y_{jk}}$	$\frac{1}{y_{ij}}$	$\frac{1}{y_{jk}}$	$\frac{y_{jk}}{y_{ij}}$	$\frac{y_{ij}}{y_{jk}}$	$\frac{y_{jk}^2}{y_{ij}}$	$\frac{y_{ij}^2}{y_{jk}}$	$\frac{1}{y_{jk}(1-y_{ij})}$	$\frac{1}{y_{ij}(1-y_{jk})}$	1	y_{ij}	y_{jk}
<i>qq̄ → qq̄</i>												
++ → ++++	1	0	0	0	0	0	0	0	0	0	0	0
++ → +-+	1	-2	-2	1	1	0	0	0	0	2	0	0
+- → +++-	1	0	-2	0	1	0	0	0	0	0	0	0
+- → +--	1	-2	0	1	0	0	0	0	0	0	0	0
<i>qg → qgg</i>												
++ → ++++	1	0	0	0	0	0	0	1	0	0	0	0
++ → +-+	1	-2	-3	1	3	0	-1	0	0	3	0	0
++ → +++-	0	0	-1	0	-1	0	-1	1	0	0	0	0
+- → +++-	1	0	-3	0	3	0	-1	0	0	0	0	0
+- → +--	1	-2	0	1	0	0	0	1	0	0	0	0
+- → +-+	0	0	-1	0	-1	0	-1	1	0	0	0	0
<i>gg → ggg</i>												
++ → ++++	1	0	0	0	0	0	0	1	1	0	0	0
++ → +-+	1	-3	-3	3	3	-1	-1	0	0	3	1	1
++ → +++-	0	0	-1	0	-1	0	-1	1	0	0	0	0
++ → -++	0	-1	0	-1	0	-1	0	0	1	0	0	0
+- → +++-	1	0	-3	0	3	0	-1	0	1	0	0	0
+- → +--	1	-3	0	3	0	-1	0	1	0	0	0	0
+- → +-+	0	0	-1	0	-1	0	-1	1	0	0	0	0
+- → -+-	0	-1	0	-1	0	-1	0	0	1	0	0	0
<i>qg → qq'q'</i>												
++ → +++-	0	0	0	0	0	0	1	0	0	0	0	0
++ → +-+	0	0	1	0	-2	0	1	0	0	0	0	0
+- → +++-	0	0	1	0	-2	0	1	0	0	0	0	0
+- → +-+	0	0	0	0	0	0	1	0	0	0	0	0
<i>gg → gq̄q</i>												
++ → +++-	0	0	0	0	0	0	1	0	0	0	0	0
++ → +-+	0	0	1	0	-2	0	1	0	0	0	0	0
+- → +++-	0	0	1	0	-2	0	1	0	0	0	0	0
+- → +-+	0	0	0	0	0	0	1	0	0	0	0	0

Table 5: Table of coefficients for helicity-dependent sector antenna functions. By the C and P invariance of QCD, the same expressions apply with $+ \leftrightarrow -$, $q \leftrightarrow \bar{q}$. All other antennae are zero. These are the default assignments in VINCIA. The finite terms are chosen so that the antennae are positive on all of final-state phase space.

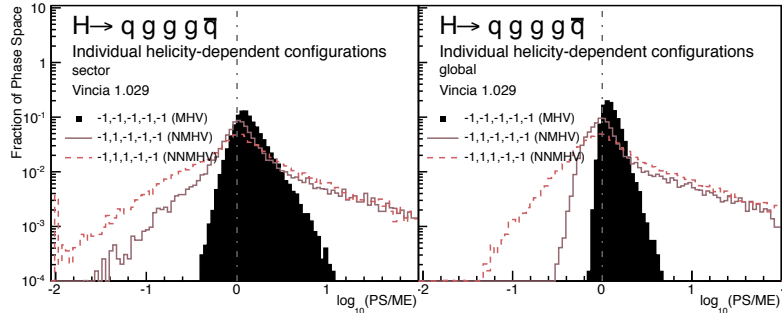


Figure 1: Accuracy of individual configurations in the shower approximation compared to helicity-dependent LO matrix elements for $H \rightarrow qggg\bar{q}$. Distributions of $\log_{10}(\text{PS}/\text{ME})$ in a flat phase-space scan, normalized to unity.

4 Results

4.1 Comparison to Matrix Elements

In order to examine the quality of the approximation furnished by a shower based on the antennae derived above, independently of the shower code, we follow the approach used for global and sector unpolarized antennae in [7, 9, 20, 22]. We use RAMBO [23] (an implementation of which has been included in VINCIA) to generate uniformly distributed 4-, 5-, and 6-parton phase-space points. At each phase-space point, we use MADGRAPH v. 4.4.26 [18] and the HELAS libraries [19] to evaluate the leading-color, helicity-dependent matrix element. As with matching, the MADGRAPH code has been modified to extract individual helicity configurations and color structures.

For each phase-space point and helicity configuration, the corresponding antenna shower approximation to the matrix element is then computed. This is done by using a clustering algorithm that contains the exact inverse of the default VINCIA $2 \rightarrow 3$ kinematics map [13]. This $3 \rightarrow 2$ clustering procedure is continued until the desired matched order is reached. At each step in the kinematic clustering procedure, the antennae corresponding to all possible intermediate spins that could have been generated by the helicity-dependent shower are summed over. To match the global shower to matrix elements requires summing over all possible kinematic clustering histories. The sector shower, by contrast, has a unique kinematic history. To determine which sector is clustered in each step, a partitioning variable must be used. Our default sector decomposition prescription is based on the variable $Q_{s_j}^2$, defined in [7]. The three-parton configuration with the smallest value of $Q_{s_j}^2$ gets clustered. This procedure produces the shower approximation to the matrix element as a nested product of helicity-dependent antenna functions.

To compare the shower to matrix elements we will consider Z and H decays to quarks with additional radiation. We begin by comparing directly the helicity matrix elements to the helicity-shower approximation. In the comparison, we will organize the helicity configurations by their complexity. We refer to processes with the maximum number of like helicities with the standard name of maximally helicity violating (MHV). Processes with one spin flip with respect to MHV we refer to as next-to-MHV (NMHV), and similarly for more complex spin configurations. We will see that the helicity-dependent shower approximates the MHV helicity matrix elements very well, and the accuracy of the shower decreases as the helicity structure becomes more complicated. However, NMHV and higher helicity configurations are subdominant contributions to the spin-summed process, in general. Thus, when summing over spins, we expect the helicity shower to have comparable accuracy to

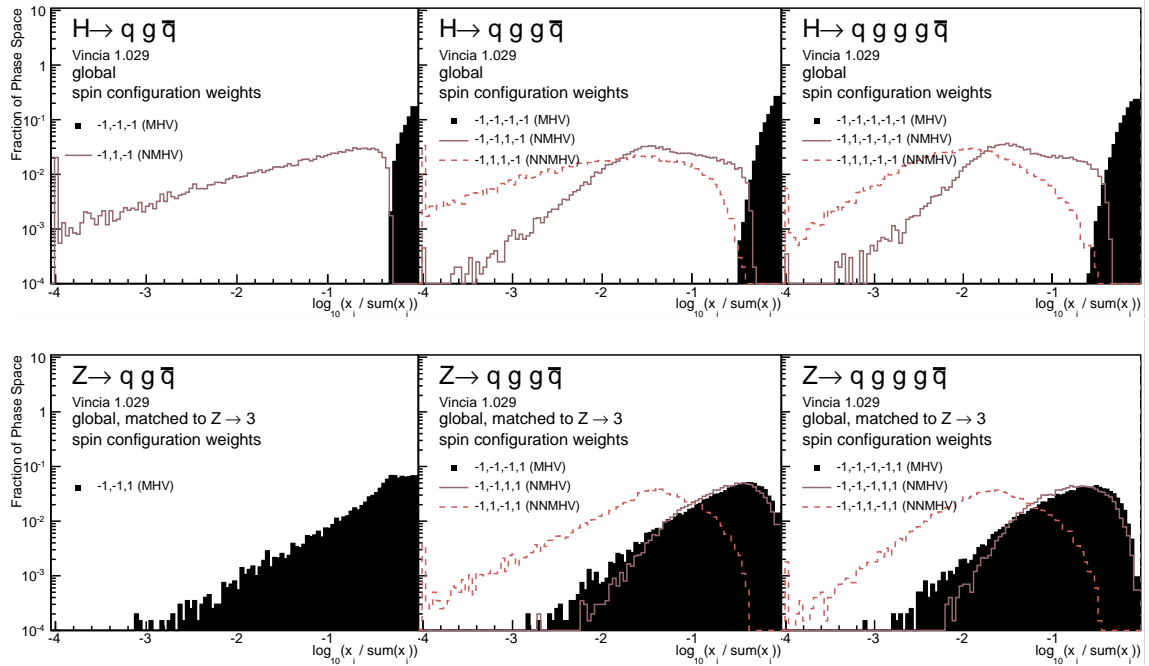


Figure 2: Relative weight of some specific helicity configurations in the global shower approximation to LO matrix elements for $H \rightarrow q\bar{q} + \text{gluons}$ (above) and $Z \rightarrow q\bar{q} + \text{gluons}$ (below). The sector shower displays basically the same structure, in particular the same hierarchy MHV, NMHV, NNMHV. The sum $\sum x_i$ runs over all helicity configurations with the same helicities for $q\bar{q}$ and includes, in some cases, configurations that are not being plotted. Distributions of $\log_{10}(\text{PS}/\text{ME})$ in a flat phase-space scan, normalized to unity.

the spin-summed matrix element as for MHV configurations.

In fig. 1, we compare the parton shower approximation to the matrix element for the process $H \rightarrow qggg\bar{q}$ for different spin configurations of the gluons. As expected, the MHV configuration is best approximated by the helicity shower. Also, note that the global shower is more accurate than the sector shower, for the same spin configuration. Note, however, that flat phase space is unphysical, and the effective accuracy of the shower will actually be significantly better for realistic phase-space weighting.

It is interesting to compare the relative weight of the spin configurations generated by the helicity shower. In fig. 2 we plot the ratio of the matrix element approximation from the global helicity shower to the spin-summed matrix element approximation for both H and Z decay processes. The corresponding plots for the sector shower are similar. As expected, the MHV-type matrix elements are most of the spin-summed result. This is most evident in the plot for the H decay. Because the H is a scalar, the helicity of the quark decay products must be the same and so the MHV configuration consists of all quarks and gluons with the same helicity. By contrast, because the Z is a vector, the helicities of the quarks are different and so the MHV configuration already has one spin flipped.

We now compare spin-summed matrix elements to summing over spin configurations in the helicity shower and to an unpolarized antenna shower as in [7, 9]. As mentioned earlier, we expect some level of accuracy improvement with the spin-summed helicity shower as compared to the unpolarized shower. In the helicity shower, some spin configurations are not allowed to contribute, while the unpolarized shower gives equal weight to every possible spin configuration. To compare the two approaches, we will focus on the singular behavior of the shower, as the non-singular terms are arbitrary anyway. To do this, we will demand that at least one pair of adjacent partons has a small invariant; namely, we require that $y_{ij} < 0.01$ for neighbors i and j . The ratio of the parton shower approximation to the matrix elements are plotted in fig. 3 for the global shower and fig. 4 for the sector shower. Note that there is a small decrease in the width of the distributions for the spin-summed helicity shower with respect to the unpolarized shower, especially at higher multiplicities.

However, we do not expect that the helicity-dependent shower is more accurate than the unpolarized shower when considering matrix elements with gluon splitting to quarks. From tab. 3 and tab. 5, the gluon splitting antennae reproduce the unpolarized antennae both by summing over the final spins for a given initial spin configuration as well as summing over the initial spins for a final spin configuration. This implies that, for example, the approximation to the spin-summed matrix element for the process $H \rightarrow q\bar{q}q'\bar{q}'$ is exactly the same in the helicity shower as the unpolarized shower (up to non-singular terms). We therefore do not include comparisons between the two.

It is also useful to see the dependence of the accuracy of the shower on the choice of arbitrary finite terms in the antennae. In fig. 5 we plot the spin-summed helicity shower with the default, MIN and MAX definitions of the non-singular terms in the antennae from section 3. Even with these rather extreme choices for the finite terms in the antennae (especially for MAX), the shower still gives a good approximation to the matrix elements. As the multiplicity increases, the finite terms become less important.

The previous plots served to illustrate the behavior of the shower expansions, starting from 3 partons and comparing to the tree-level matrix element result at each successive multiplicity. However, in the GKS matching algorithm implemented in VINCIA, the matrix-element corrections are actually performed sequentially, order by order. That is, the correction to 4 partons is applied before the evolution goes on to 5 partons, and so on. In that context, what is relevant for, say, the 6-parton correction factor is therefore not the pure shower expansion but rather the approximation obtained from a single branching step starting from the 5-parton matrix element. Moreover, most of the previous plots focused on the shower-dominated regions of phase-space. In real life, events will

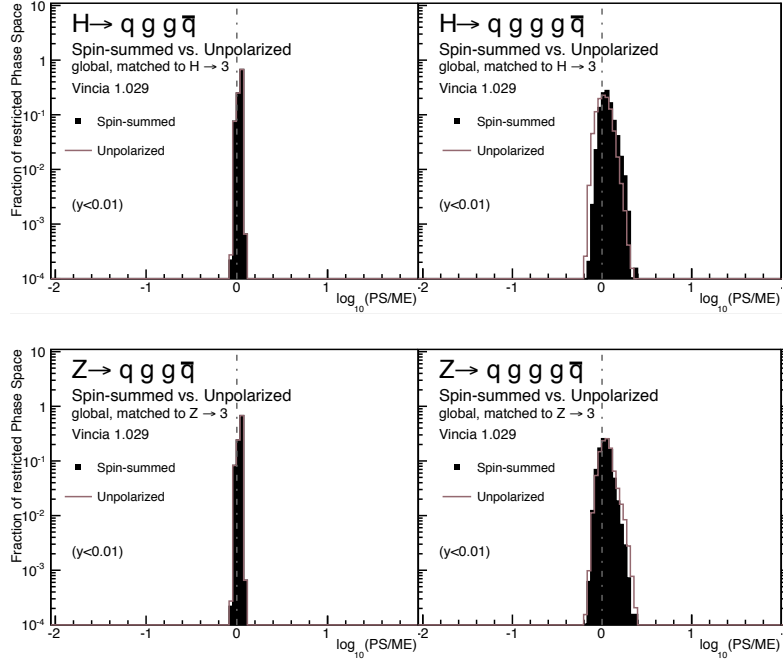


Figure 3: Global showers. Spin-summed helicity-dependent and unpolarized shower approximations compared to LO matrix elements for $H \rightarrow q\bar{q} + \text{gluons}$ (above) and $Z \rightarrow q\bar{q} + \text{gluons}$ (below). Distributions of $\log_{10}(\text{PS}/\text{ME})$ in a flat phase-space scan, normalized to unity, with hard configurations excluded.

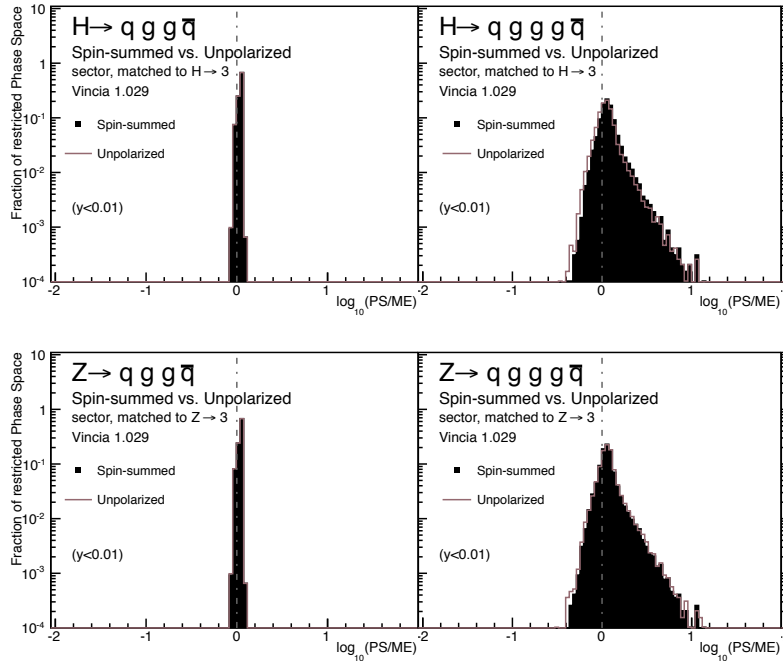


Figure 4: Sector showers. Spin-summed helicity-dependent and unpolarized shower approximations compared to LO matrix elements for $H \rightarrow q\bar{q} + \text{gluons}$ (above) and $Z \rightarrow q\bar{q} + \text{gluons}$ (below). Distributions of $\log_{10}(\text{PS}/\text{ME})$ in a flat phase-space scan, normalized to unity, with hard configurations excluded.

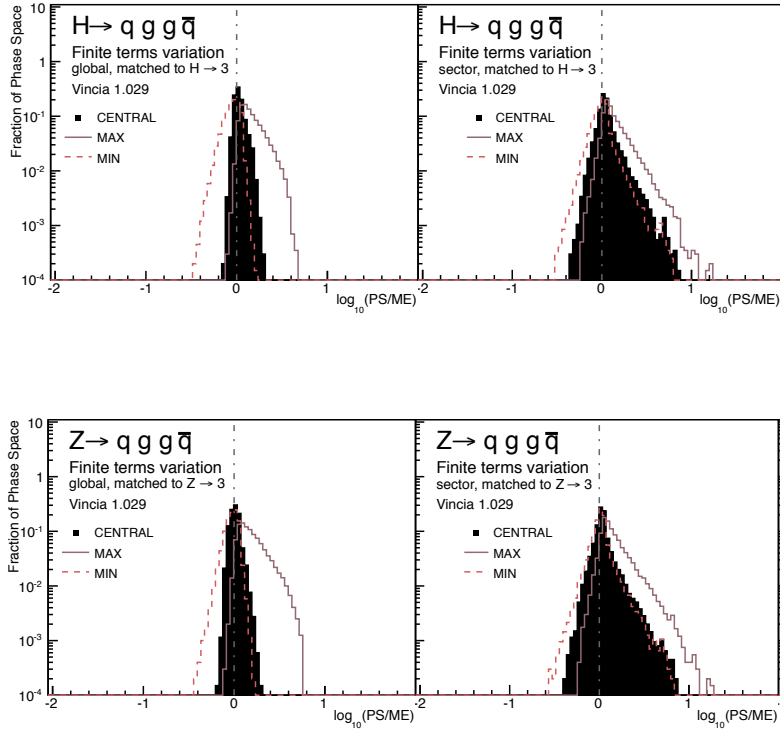


Figure 5: Central, MIN and MAX variations of the antennae for the global and sector shower approximations to LO matrix elements for $H \rightarrow q\bar{q} + \text{gluons}$ and $Z \rightarrow q\bar{q} + \text{gluons}$. Distributions of $\log_{10}(\text{PS}/\text{ME})$ in a flat phase-space scan, normalized to unity.

be obtained with a continuous distribution of scales, from hard to soft. To illustrate the distribution of correction factors in actual VINCIA runs, without any phase-space cuts (apart from the hadronization scale), we make use of the fact that VINCIA stores several internal diagnostics histograms during running, when the verbosity parameter `Vincia:verbose` is set to values ≥ 2 . These make use of PYTHIA’s simple histogramming utility and can be printed at the end of a run by invoking the command `VinciaShower::printHistos()`. Part of these diagnostics histograms contain the ME/PS weight ratios for both trial and accepted branchings. The latter accurately reflects the distribution of ME/PS correction factors for each physical branching that occurs in the evolution. Note, though, that the ratio is here inverted, from PS/ME to ME/PS; above, we were interested to know whether the shower over- or under-counted the matrix element. For GKS matching, we are interested in the size of the correction factor, which is proportional to ME/PS.

Fig. 6 shows a compilation of such plots, for $Z \rightarrow 4, 5,$ and 6 partons, using the default global helicity-dependent showers. The left-hand pane shows gluon-emission distributions, the three curves representing $Z \rightarrow q\bar{q}gg$, $Z \rightarrow q\bar{q}ggg$, and $Z \rightarrow q\bar{q}gggg$, respectively. The central dashed line represents perfect agreement (the matrix-element correction factor is unity), while the two solid lines represent a factor two deviation in each direction. Despite the fact that we are now including hard as well as soft branchings and that the matching factors now also include components designed to absorb the subleading-color corrections [9], the distributions are still quite narrow. Importantly, we do not observe any substantial degradation of the correction factor with multiplicity, suggesting that the GKS matching strategy is quite stable.

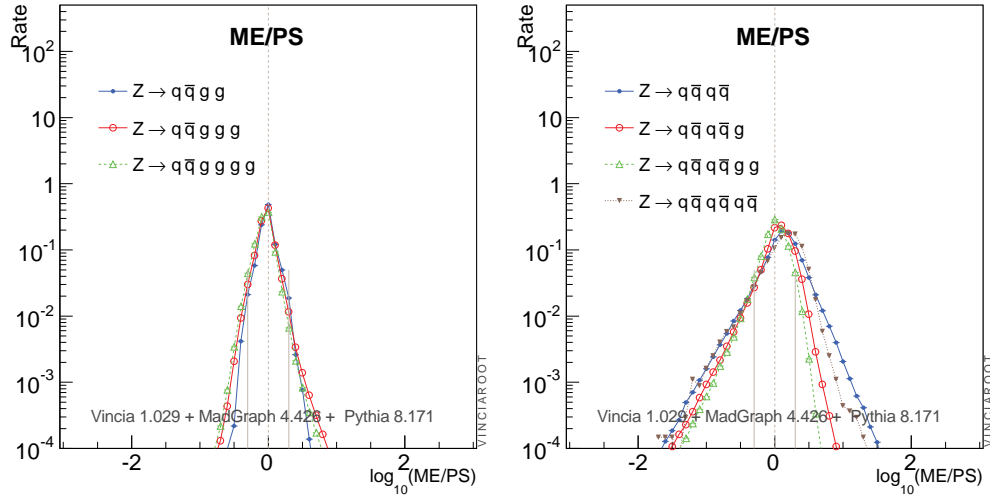


Figure 6: Global showers. Distributions of the ME/PS correction factors in actual VINCIA runs, for decays of unpolarized Z bosons to massless quarks, using helicity-dependent antenna functions. *Left:* correction factors for gluon emission. *Right:* correction factors for events involving $g \rightarrow q\bar{q}$ splittings.

In the right-hand pane of fig. 6, we show the equivalent distributions for events involving $g \rightarrow q\bar{q}$ splittings. (In absolute terms, these events are of course less frequent than the gluon-emission ones, but we here normalize all plots to unity.) As expected, the distributions are broader, reflecting the fact that the uncorrected cascade is less precise for this type of branchings, due to the less singular nature of the $g \rightarrow q\bar{q}$ antenna functions. The consequence of this is that relatively large trial overestimates need to be used for $g \rightarrow q\bar{q}$ splittings in order that the tail of large corrections does not lead to unitarity violations. Nevertheless, the method appears to remain stable even after multiple $g \rightarrow q\bar{q}$ splittings (the dotted curve shows the comparison to the $Z \rightarrow qq\bar{q}\bar{q}$ matrix element).

The effect of the GKS matrix-element corrections is to transform the distributions in fig. 6 back to delta functions (corrected PS = ME) at each order. In particular the amount and distribution of $g \rightarrow q\bar{q}$ splittings in the matrix-element corrected cascade should thus be substantially more accurate than would be the case in the pure shower.

4.2 Speed

A central point of the helicity-based approach presented here is that high computational speeds can be obtained, even when including matching to quite large partonic multiplicities. There are essentially three important reasons for this:

- The initialization time is essentially zero. In the GKS matching scheme [9], only the Born-level cross section needs to be precomputed, and only a Born-level fixed-order phase-space generator needs to be initialized, resulting in essentially vanishing initialization times (of order fractions of a second). This is in contrast to slicing-based strategies like L-CKKW [2, 3], MLM [4], and others [5, 24] for which the inclusive cross section for each matched multiplicity must be precomputed and a corresponding n -parton phase-space generator initialized (“warmed up”) before event generation can begin.
- In all (unweighted) fixed-order calculations, and consequently also in slicing-based matching strategies, one faces the problem that QCD amplitudes beyond the first few partons have quite

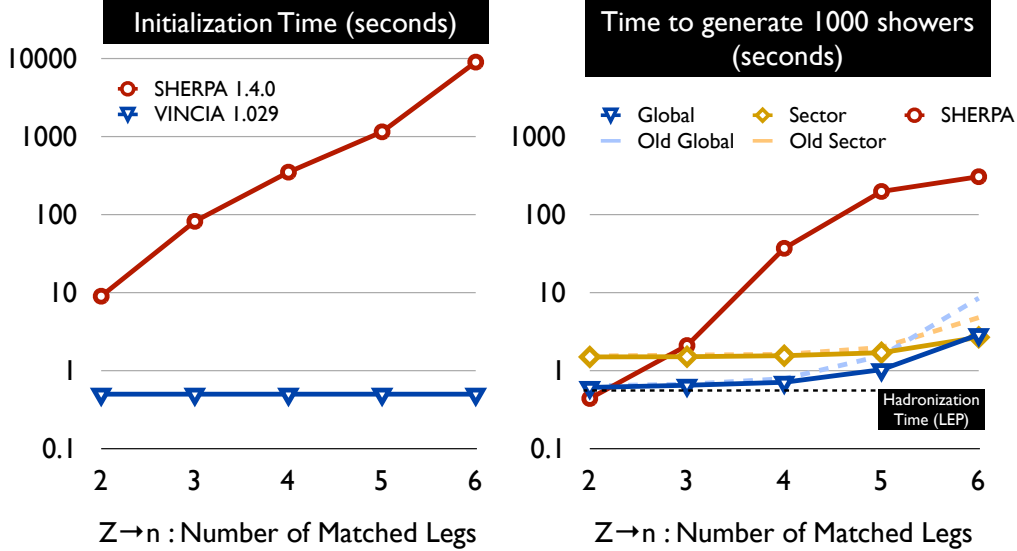


Figure 7: Comparison of computation speeds between SHERPA version 1.4.0 [27] and VINCIA 1.029 + PYTHIA 8.171, as a function of the number of legs that are matched to matrix elements, for hadronic Z decays. *Left:* initialization time (to precompute cross sections, warm up phase-space grids, etc, before event generation). *Right:* time to generate 1000 parton-level showered events (not including hadronization), with VINCIA’s global and sector showers shown separately, with and without (“old”) helicity dependence. For comparison, the average time it takes to hadronize such events with PYTHIA’s string hadronization model [28] is shown as a dashed horizontal line. Further details on the setup used for these runs are given in the text.

complicated structures in phase space. This means that even fairly clever multi-channel strategies have a hard time achieving high efficiency over all of it. In GKS, this problem is circumvented by generating the phase space by a (trial) shower algorithm, which is both algorithmically fast and is guaranteed to get at least the leading QCD singularity structures right¹. Since those structures give the largest contributions, the fact that the trials are less efficient for hard radiation has relatively little impact on the overall efficiency². Combining this with the clean properties of the antenna phase-space factorization and with matching at the preceding orders, the trial phase-space population at any given parton multiplicity is already very close to the correct one, and identical to it in the leading singular limits, producing the equivalent of very high matching-and-unweighting efficiencies.

- Finally, the addition of helicity dependence to the trial generation in this paper allows us to match to only a single helicity amplitude at a time, at each multiplicity. This gives a further speed gain relative to the older approach [9] in which one had to sum over all helicity configurations at each order. In addition, the MHV-type helicity configurations tend to give the dominant contribution to the spin-summed matrix element. MHV amplitudes are also those best described by the shower because they contain the maximum number of soft and collinear singularities.

The speed of the old (helicity-independent) VINCIA algorithm was examined in [7], for the process of Z decay to quarks plus showers, and was there compared to SHERPA [27], as an example of a slicing-based multileg matching implementation. In fig. 7, we repeat this comparison, including now

¹A related type of phase-space generator is embodied by the SARGE algorithm [25], and there are also similarities with the forward-branching scheme proposed in [26].

²As long as all of phase-space is covered and the trials remain overestimates over all of it, something which we have paid particular attention to in VINCIA, see [9].

the helicity-dependent VINCIA implementations as well. Needless to say, other factors play in when comparing two completely different programs such as SHERPA and VINCIA + PYTHIA. We do not attempt to account fully for differences in code structures and optimizations here, so the absolute values shown in fig. 7 should not be taken too seriously. Nonetheless, we may take the results obtained with SHERPA as representative of the scaling exhibited by slicing-based strategies in general, and that by VINCIA of multiplicative ones.

For SHERPA, we used the COMIX [29] matrix-element generator, while VINCIA’s matrix elements come from MADGRAPH 4 [18] and HELAS [19]. A matching scale of 5 GeV was imposed for all matched multiplicities in SHERPA. In VINCIA, matching is normally carried out over all of phase space; for this comparison, we limited the highest matched matrix elements to the region above 5 GeV, while lower multiplicities were still matched over all of their respective phase spaces. In both programs, bottom quarks were treated as massive, lighter ones as massless. The tests were run on a single 3.05 GHz CPU (with 4GB memory) using gcc 4.6, with O2 optimization. Hadronization and initial-state photon radiation were switched off.

The point about initialization time is clearly illustrated in the left-hand pane of fig. 7; in the CKKW-based matching strategy implemented in SHERPA, the integration of each additional higher-leg matrix element and the warm-up of the corresponding phase-space generator takes progressively more time at startup (note the logarithmic scale), while VINCIA’s initialization time is independent of the desired matching level.

In the right-hand pane of fig. 7, the time required to generate (unweighted) events in CKKW also starts by rising rapidly, but then eventually levels off and appears to saturate at ~ 6 partons. We interpret the reason for this to be that, while it still takes a long time to compute the total 6-jet cross section (reflected in the left-hand pane), the actual value of that cross section is quite small, and hence only a small fraction of the generated events will actually be of the six-jet variety. The precise behavior of course depends on the choice of matching scale.

In addition, on the right-hand pane of fig. 7, the solid VINCIA curves represent the new (helicity-dependent) formalism, for global (triangle symbols) and sector (diamond symbols) showers, respectively. The dashed curves shown in lighter shades give the corresponding results without helicity dependence. At 2 partons, i.e., without any matching corrections, we see that the VINCIA showers are currently slightly slower than the SHERPA ones. This was not the case in [7], and is due to the trial-generation machinery in VINCIA having been rewritten in a simpler form, which is slightly more wasteful of random numbers, an optimization point we intend to return to in the future. The main point of our paper, however, is the scaling with the number of additional matched legs exhibited by the helicity-dependent GKS matching formalism, which is almost flat in the sector case, and still significantly milder in the global case than for the CKKW-based SHERPA comparison.

4.3 Validation

To complete the validation of the new helicity-dependent framework, we include a set of comparisons to LEP measurements at the event-, jet-, and particle levels, respectively. These comparisons were carried out using the default settings for VINCIA 1.029, which include a slight re-optimization of the hadronization parameters in a new default tune called “Jeppsson 5”, with parameters given in appendix B. For reference, comparisons to default PYTHIA 8.172 (with VINCIA switched off) are provided as well. In all cases, we consider hadronic decays of unpolarized Z bosons, at $E_{cm} = 91.2$ GeV, corrected for initial-state photon radiation effects, and letting particles with $c\tau > 100$ mm be stable.

All plots were made using VINCIA’s ROOT-based runtime displays [9, 30], which can be saved

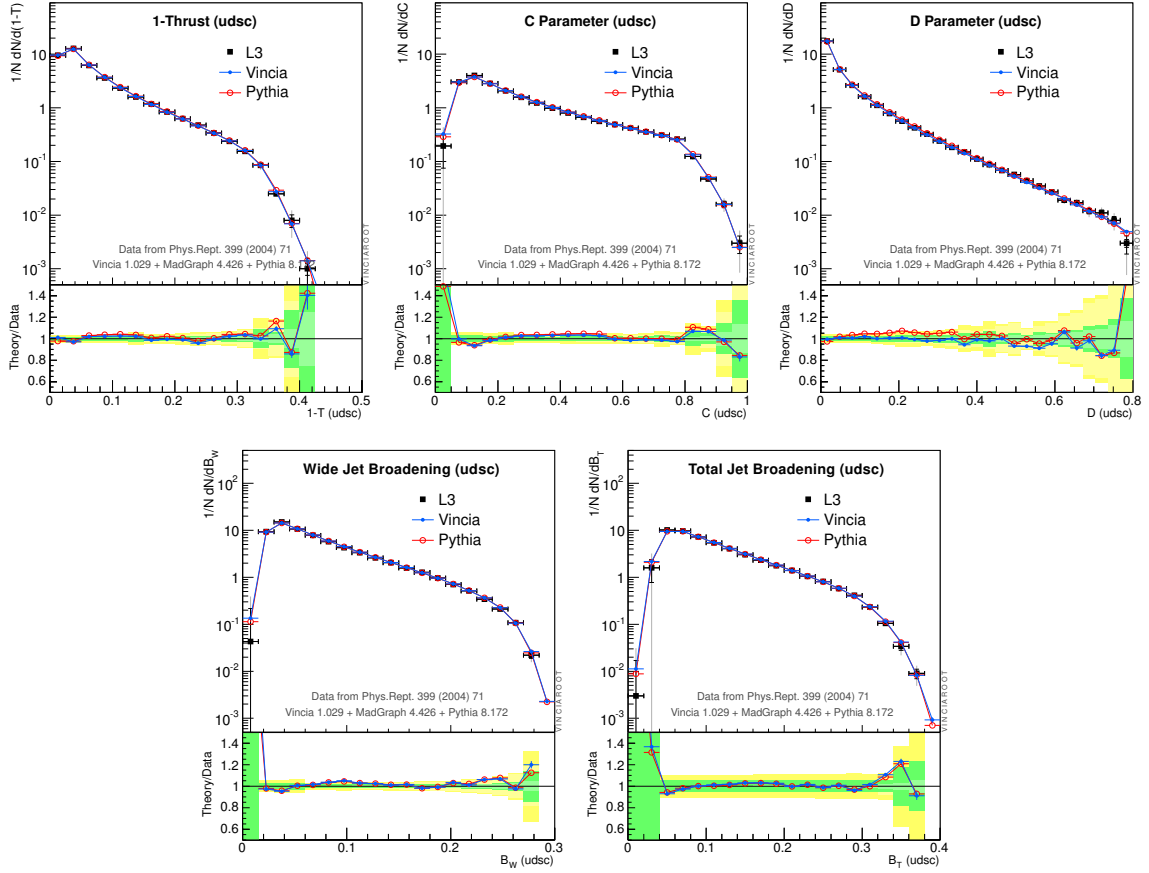


Figure 8: Event shapes measured in light-flavor tagged events by the L3 experiment at the Z pole [31], compared to default VINCIA 1.029 and PYTHIA 8.172.

to graphics files using the `VinciaRoot::saveDisplays()` command. VINCIA is shown with solid (blue) lines and filled dot symbols. PYTHIA is shown with solid (red) lines and open circle symbols. Experimental data is shown with black squares and black crosshairs that correspond to one standard deviation. Where applicable, two crosshairs are overlotted on one another, corresponding to statistical-only and total (stat + sys, summed in quadrature) uncertainties. Light-gray vertical extensions of the crosshairs illustrate two standard deviations. The uncertainties on the MC runs are statistical only, and are shown at the two-sigma level, to be conservative. In the ratio panes below the main plots, we show theory/data; the inner (green) shaded bands show one-sigma deviation contours, the outer (yellow) ones two-sigma contours³.

Since we only apply the helicity-dependent formalism to massless partons, we begin by focusing on light-flavor tagged events. A very useful such set of measurements was performed by the L3 collaboration [31]. In fig. 8, we show how default VINCIA 1.029 compares to that data set, for the Thrust, C, and D parameters (top row), and for the Wide and Total Jet Broadening (bottom row), see [31] for definitions. No significant deviations are observed, hence the code passes this validation step. As in previous VINCIA studies [7,9] (and PYTHIA ones [32–34]), however, one should note that this

³For completeness, an additional very slight shading variation inside each band shows the purely statistical component, where applicable.

agreement comes at the price of using a rather large value for $\alpha_s(M_Z)$,

$$\alpha_s(M_Z) = 0.139 , \quad (17)$$

which, with one-loop running (the default in VINCIA), corresponds to a five-flavor Λ_{QCD} value of

$$\Lambda_{\text{QCD}}^{(5)} = 0.25 \text{ GeV} . \quad (18)$$

In a pure parton shower, such a large value could perhaps be interpreted as an attempt to compensate for missing hard higher-multiplicity matrix-element corrections. With VINCIA, however, we find that such an interpretation cannot be the whole story, since the default VINCIA settings include LO matrix-element corrections through $Z \rightarrow 5$ partons.

In our view, there are two factors contributing to the large α_s value favored by the PYTHIA and VINCIA tunings. Firstly, the α_s value extracted from a Monte Carlo tuning is not guaranteed to be directly interpretable as an $\overline{\text{MS}}$ value. Indeed, CMW argued [35] that a rescaling of the effective Λ_{QCD} value by a factor 1.57 (for 5 flavors) is appropriate when translating from $\overline{\text{MS}}$ to a coherent Monte-Carlo shower scheme. With the caveat that the original CMW argument was based on two-loop running while VINCIA currently defaults to one-loop running, a naive application to the value found above would reduce the equivalent $\overline{\text{MS}}$ value to:

$$\Lambda_{\text{QCD}}^{(5)\overline{\text{MS}}} \sim \frac{0.25 \text{ GeV}}{1.57} = 0.16 \text{ GeV} , \quad (19)$$

corresponding to a (one-loop) value for $\alpha_s(M_Z)$ of ~ 0.129 . Secondly, this still rather high value should then be seen in the context of an LO+LL extraction. The inclusion of the full NLO correction to $Z \rightarrow 3$ jets, which is the topic of a forthcoming paper [36], generates additional order 10% corrections to hard radiation, which should bring the extracted value further down, and the expectation is that the tuned value would then be in accordance with other NLO extractions. We shall return to this issue in more detail in [36].

Passing now from event shapes to jets, the first 5 panes of fig. 9 show a comparison to the 2-, 3-, 4-, 5-, and 6-jet resolution scales measured by the ALEPH collaboration [37] (now including also $Z \rightarrow b\bar{b}$ events), using the Durham k_T clustering algorithm [39], with distance measure

$$y_{ij} = \frac{2\min(E_i^2, E_j^2)(1 - \cos\theta_{ij})}{E_{\text{vis}}^2} , \quad (20)$$

for which we use the FASTJET implementation [40]. Formally, E_{vis} is the total visible energy, but since the ALEPH data were corrected for the distortions caused by neutrinos escaping detection, we here include neutrinos in the inputs passed to FASTJET. Hard scales have values $\ln(y) \sim 0$ and hence appear towards the left edge of the plots in fig. 9, while soft scales appear towards the right-hand edges. Non-perturbative effects are expected to dominate below roughly 1 GeV, corresponding to $\ln(1/y) \sim \ln(91^2/1^2) \sim 9$. Above this scale, i.e. in the perturbative region, we observe no disagreement between the ALEPH data and VINCIA. (Note that the distributions are affected by the kinematics of B decays starting already from $\ln(1/y) \sim \ln(91^2/5^2) \sim 5.8$, but these decays are modeled adequately by PYTHIA, and hence do not trouble this comparison. The feature at $\ln(1/y) \sim 10$ in the 5- and 6-jet resolutions corresponds to clustering scales below 1 GeV and hence is likely to be associated with a combination of string breaking and hadron decays.)

As a verification that the perturbative mass corrections for heavy quarks have not been altered by the new implementation, the last pane in fig. 9 shows the ratio of b - to light-quark 3-jet resolutions

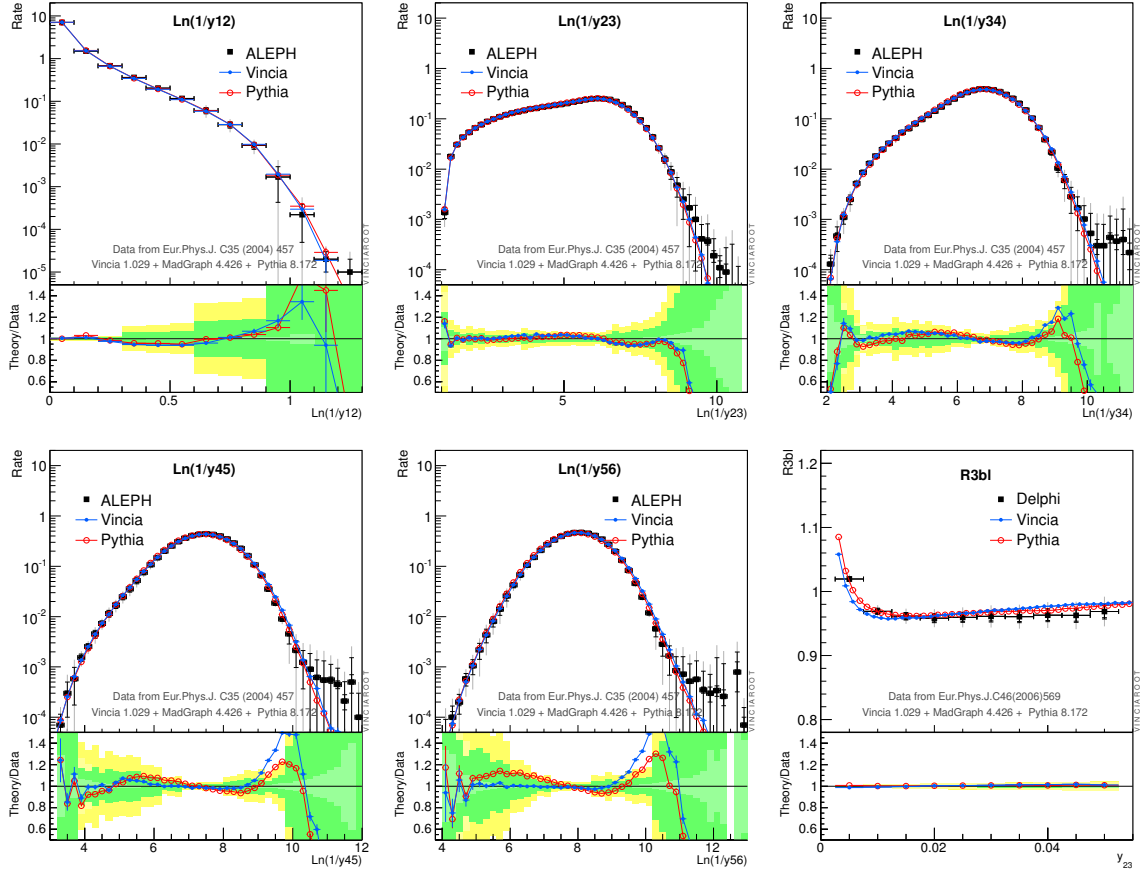


Figure 9: From Top Left: Jet resolution distributions measured by the ALEPH experiment at the Z pole [37]. Bottom Right: The ratio of 3-jet rates in b - vs. light-flavor tagged events, as a function of Durham y_{23} , measured by the DELPHI experiment [38]. Comparisons to default VINCIA 1.029 and PYTHIA 8.172.

measured by DELPHI [38], which also appeared as one of the validation plots in our dedicated study of mass effects [20]. The distribution is essentially unchanged with respect to the previous study, and retains its non-trivial shape.

Lastly, we turn to distributions at the individual particle level. The top row of fig. 10 shows the charged-particle multiplicity and momentum spectra, again for light-flavor tagged L3 events [31], with no significant deviations between VINCIA and the data. (The feature around $\ln(1/x) \sim 6$ corresponds to momentum scales close to the pion mass and is also seen in standalone PYTHIA, hence we interpret it as an issue with the non-perturbative hadronization model.)

The bottom row of fig. 10 shows the relative fractions of various identified particles, normalized by the average charged-particle multiplicity. The experimental numbers are here labeled “LEP” and represent our own estimates, using a combination of inputs from PDG [41] and HEPDATA [42]. The two leftmost panes show meson and baryon fractions, respectively. The meson fractions are somewhat better described than the baryon ones, and slightly different tuning priorities are evident between PYTHIA and VINCIA, but in no case do we see a significant deviation from the data. One remark is worth making, though, that the production of strange and multi-strange baryons tends to be at the lower limit of what is allowed by the data. We have addressed this by removing any strange-baryon suppression relative to light-flavor ones in the string-fragmentation flavor selection, but note

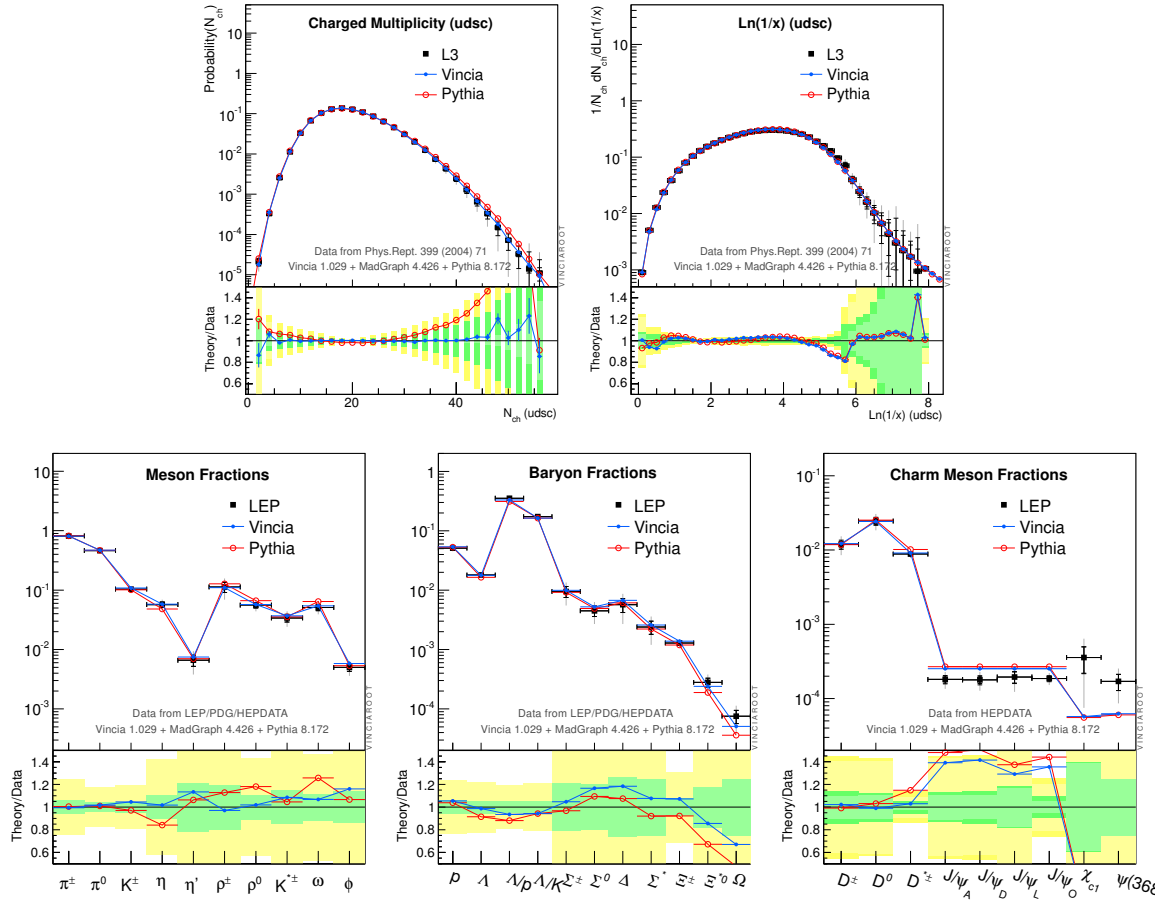


Figure 10: Top Row: Inclusive charged-particle multiplicity and momentum spectra in light-flavor tagged events measured by the L3 experiment at the Z pole [31]. Bottom Row: Meson, Baryon, and Charm-Meson fractions (normalized to the average charged multiplicity). Comparisons to default VINCIA 1.029 and PYTHIA 8.172.

that the data might even prefer a slight enhancement, which is currently not a technical possibility in PYTHIA.

As an additional piece of information less relevant to the study performed here, the last pane of fig. 10 shows a comparison to charm meson fractions. Though the total amount of charm meson production is reasonably well described, there appears to be a slight overproduction of D^* mesons in PYTHIA, and both VINCIA and PYTHIA exhibit an excess of J/ψ resonances (the four data points correspond to each of the four LEP experiments) and an underproduction of χ_{c1} and $\psi(3685)$. Especially the latter rare states are certainly not expected to be perfectly described out of the box, and hence we mostly include this comparison as a hint of where future improvements might be useful.

Finally, we should also mention that the code performs several internal self-consistency checks during initialization. In particular, the soft and collinear limits of all antenna functions are checked against the respective eikonal and (helicity-dependent) Altarelli-Parisi kernels, and a verification is made that the antenna functions remain positive over all of the physical phase space.

5 Conclusions

Our development of a helicity-based shower in VINCIA shows that significant speed gains are obtained when matching to helicity matrix elements as compared to matching an unpolarized shower to spin-summed matrix elements. One reason for this is that the MHV-type helicity configurations tend to be the dominant contribution to the spin-summed matrix element. MHV amplitudes are also those best described by the shower because they contain the maximum number of soft and collinear singularities. In addition, the intrinsic accuracy of the helicity shower is increased with respect to the unpolarized shower for essentially the same reason.

There are several directions in which the helicity formalism developed here can be extended in VINCIA. First, as mentioned in section 2.3, mass effects can be included using the phase-space maps from [20] and the massive splitting functions from [21]. In the massive case, the spin of a particle does not have an unambiguous definition and so one must take care in defining the spin in a consistent manner. We advocate for defining the spin of a massive fermion by its chirality; however, the spin can also be defined by a projection onto a reference vector. Both have subtleties: chirality is Lorentz invariant, but can flip from mass insertions. Using a reference vector to define spin breaks Lorentz invariance so one must be careful to use the same reference vector for all calculations so that the final result, when summed over spins, is Lorentz invariant. Our advocacy for using chirality is based on its Lorentz invariance as well as its importance in weak decays. Mass effects are particularly important in top quark decays where all of these effects can be studied.

While there are many subtleties in extending VINCIA to include initial state radiation (ISR) for hadron collisions [43] or next-to-leading order (NLO) matching [36], implementing the helicity shower within these frameworks should be straightforward. The helicity antennae described here would work in the initial state as well, with the possible caveat that the finite terms in the antennae might need to be changed to guarantee positivity in the initial state phase space. Matching the shower in hadron collisions to helicity amplitudes would maintain the speed gains illustrated here. However, the matching procedure would have to be changed because, for hadron collisions, it would no longer be practical to develop a complete library of matrix elements to which to match. A hybrid approach in which matrix elements are computed dynamically as well as extracting some matrix elements from libraries would be necessary. A similar procedure exists in SHERPA, where tree-level helicity amplitudes are computed from Berends-Giele [44] recursion relations in COMIX [29] and by Feynman diagrams in AMEGIC++ [45]. Matching to NLO matrix elements would require utilizing the libraries from BLACKHAT [46], for example, in which the individual helicity components to the process can be extracted. A recent study [47] showed that the most efficient method for calculating helicity amplitudes depends on the spin configuration as well as the number of external particles.

Acknowledgments

This work was supported in part by the European Commission (HPRN-CT- 200-00148), FPA2009-09017 (DGI del MCyT, Spain) and S2009ESP-1473 (CA Madrid). J.J. L-V has been supported by a MEC grant, AP2007-00385 and as a CERN visitor at the Theory Division. He wants to thank its hospitality, and also the groups at CEA Saclay IPhT and Lund. A. L. is supported by the US Department of Energy under cooperative research agreement DE-FG02-05ER41360 and supported in part by the U.S. National Science Foundation, grant NSF-PHY-0969510, the LHC Theory Initiative, Jonathan Bagger, PI. A. L. also wishes to thank the CERN Theory Division and the CEA Saclay IPhT for their hospitality during recent visits.

A Antenna Construction

A.1 Construction of Unpolarized Global Antennae

In this appendix, we present the construction of the unpolarized global antennae as an illustration of the more general procedure for determining the helicity-dependent global antennae. To determine the singular terms in spin-dependent global antenna functions, it suffices to consider the $gg \rightarrow ggg$ emission and $gg \rightarrow g\bar{q}q$ splittings only. The gluon splitting antennae are the same as their sector counterparts, decreased by a factor of 2 because of the two antennae which contribute. The global gluon emission antennae are significantly more complicated. We first use the constraints described in section 3.1 to determine the spin-summed global antenna functions to see how they can be used to reproduce familiar results. The procedure will naturally generalize to the spin-dependent case.

To analyze the collinear limits of two gluons j and k it suffices to consider the configuration of four ordered gluons i, j, k and l . There are two splittings that contribute to the collinear limit of j and k :

$$\begin{aligned} i(\hat{j}\hat{l}) &\rightarrow i(jkl), \\ (\hat{i}\hat{k})l &\rightarrow (ijk)l. \end{aligned}$$

Here, the parentheses associate the $2 \rightarrow 3$ splitting in the gluon configuration. The singular terms of the antenna for the first splitting can be written as

$$\hat{j}\hat{l} \rightarrow jkl = \frac{2}{y_{jk}y_{kl}} + \frac{f_1(y_{kl})}{y_{jk}} + \frac{f_2(y_{jk})}{y_{kl}}, \quad (21)$$

for some polynomials f_1 and f_2 . Similarly, the second splitting can be expressed as

$$\hat{i}\hat{k} \rightarrow ijk = \frac{2}{y_{ij}y_{jk}} + \frac{f_3(y_{jk})}{y_{ij}} + \frac{f_4(y_{ij})}{y_{jk}}, \quad (22)$$

for some polynomials f_3 and f_4 . Note that by Bose symmetry, $f_1 = f_3$ and $f_2 = f_4$. Further, all f_i s are actually equal because of the symmetric initial and final splitting states. Thus, we will replace $f_i \equiv f$.

Now, consider the limit where $j \parallel k$. In this limit, we set $y_{ij} = z$ and $y_{kl} = 1 - z$. Then, the two antennae can be written as

$$\hat{j}\hat{l} \rightarrow jkl = \frac{1}{y_{jk}} \left[\frac{2}{1-z} + f(1-z) \right], \quad (23)$$

$$\hat{i}\hat{k} \rightarrow ijk = \frac{1}{y_{jk}} \left[\frac{2}{z} + f(z) \right]. \quad (24)$$

Without loss of generality, we can write $f(z)$ in the form

$$f(z) = (-2 - \alpha) + \alpha_1 z + \alpha_2 z^2, \quad (25)$$

for some coefficients α , α_1 and α_2 . For consistency, the sum of these splitting amplitudes must reproduce the Altarelli-Parisi splitting function:

$$P_{gg \leftarrow g}(z) = 2 \left[\frac{1-z}{z} + \frac{z}{1-z} + z(1-z) \right] = \left[\frac{2}{1-z} + f(1-z) \right] + \left[\frac{2}{z} + f(z) \right]. \quad (26)$$

This requirement enforces $\alpha_2 = -1$ and $\alpha_1 = 1 + 2\alpha$ so that $f(z) = (-2 - \alpha) + (1 + 2\alpha)z - z^2$. Note that the GGG partitioning of global antenna [17] corresponds to $\alpha = 0$ while the ARIADNE partitioning [48, 49] corresponds to $\alpha = 1$. However, both are special cases of a one-parameter family of possibilities.

Positivity of the splitting function in the singular regions can be studied by taking, for example, the limit of the antenna $\hat{i}\hat{k} \rightarrow ijk$ where $y_{jk} \rightarrow 0$ and $y_{ij} \rightarrow 1$. In this limit, for the antenna to be non-negative, the function f must satisfy $2 + f(1) \geq 0$ or that $\alpha \geq 0$. Then, the global antenna for gluon emission is

$$a(gg \rightarrow ggg) = \frac{2}{y_{ij}y_{jk}} + \frac{-2 - \alpha + (1 + 2\alpha)y_{jk} - y_{jk}^2}{y_{ij}} + \frac{-2 - \alpha + (1 + 2\alpha)y_{ij} - y_{ij}^2}{y_{jk}}. \quad (27)$$

For $0 \leq \alpha \lesssim 4$, this antenna is positive on all of final-state phase space without the addition of any non-singular terms. A table of the Laurent coefficients for generic partitioning of the unpolarized global antennae is presented in tab. 6.

\times	$\frac{1}{y_{ij}y_{jk}}$	$\frac{1}{y_{ij}}$	$\frac{1}{y_{jk}}$	$\frac{y_{jk}}{y_{ij}}$	$\frac{y_{ij}}{y_{jk}}$	$\frac{y_{jk}^2}{y_{ij}}$	$\frac{y_{ij}^2}{y_{jk}}$
$q\bar{q} \rightarrow qq\bar{q}$	2	-2	-2	1	1	0	0
$qg \rightarrow qgg$	2	-2	$-2 - \alpha$	1	$1 + 2\alpha$	0	-1
$gg \rightarrow ggg$	2	$-2 - \alpha$	$-2 - \alpha$	$1 + 2\alpha$	$1 + 2\alpha$	-1	-1
$qg \rightarrow q\bar{q}q$	0	0	$\frac{1}{2}$	0	-1	0	1
$gg \rightarrow g\bar{q}q$	0	0	$\frac{1}{2}$	0	-1	0	1

Table 6: Singular spin-summed global Laurent coefficients for the general case. $\alpha = 1$ is ARIADNE partitioning and $\alpha = 0$ is GGG partitioning.

A.2 Construction of Global Helicity-Dependent Antennae

In this appendix, we will provide details for the construction of the helicity-dependent global antennae. We will assume that the only possible non-zero $gg \rightarrow ggg$ global antennae are those which also have corresponding non-zero sector antennae. That is, antennae such as $++ \rightarrow ---$ will be set to zero⁴. Otherwise we will assume the antennae are non-zero. Without loss of generality, all possible non-zero antennae can be expressed as:

$$\begin{aligned} ++ \rightarrow +++ &= \frac{1}{y_{ij}y_{jk}} + \frac{f(y_{jk})}{y_{ij}} + \frac{f(y_{ij})}{y_{jk}}, & ++ \rightarrow +-+ &= \frac{1}{y_{ij}y_{jk}} + \frac{g(y_{jk})}{y_{ij}} + \frac{g(y_{ij})}{y_{jk}} \\ ++ \rightarrow -++ &= \frac{h_1(y_{jk})}{y_{ij}} + \frac{h_2(y_{ij})}{y_{jk}}, & ++ \rightarrow +++ &= \frac{h_2(y_{jk})}{y_{ij}} + \frac{h_1(y_{ij})}{y_{jk}} \\ +- \rightarrow +++ &= \frac{1}{y_{ij}y_{jk}} + \frac{a_1(y_{jk})}{y_{ij}} + \frac{a_2(y_{ij})}{y_{jk}}, & +- \rightarrow +-+ &= \frac{1}{y_{ij}y_{jk}} + \frac{b_1(y_{jk})}{y_{ij}} + \frac{b_2(y_{ij})}{y_{jk}} \\ +- \rightarrow +-+ &= \frac{c_1(y_{jk})}{y_{ij}} + \frac{c_2(y_{ij})}{y_{jk}}, & +- \rightarrow -+- &= \frac{c_2(y_{jk})}{y_{ij}} + \frac{c_1(y_{ij})}{y_{jk}} \end{aligned}$$

⁴These antennae must vanish by imposing the collinear limit constraints along with the positivity constraints.

for some quadratic polynomials $f, g, h_1, h_2, a_1, a_2, b_1, b_2, c_1, c_2$. All other antennae are related by C or P symmetry of QCD. Note that an antenna only has a non-zero soft limit if the helicity of the outer gluons in the antenna are conserved.

As in the unpolarized case in the previous appendix, we consider the configuration of four ordered gluons i, j, k, l and study the limit $j \parallel k$. There are 16 distinct $3 \rightarrow 4$ gluon splittings which could produce these gluons which are not related by C or P which can be used to constrain the form of the functions defined in the antennae. Demanding that the eight splitting functions above reproduce the correct soft and collinear limits for each of these $3 \rightarrow 4$ splittings leads to the requirements that:

$$\begin{aligned} f(z) &= -f(1-z) \\ a_1(z) &= b_2(z) = f(z) \\ a_2(z) &= b_1(z) = g(z) \\ h_1(z) &= c_2(z) = \frac{z^3 - 1}{1-z} - g(1-z) \end{aligned} \quad (28)$$

and that the functions $h_2(z)$ and $c_1(z)$ are unconstrained. One example of the constraints is given by, say, $+++ \rightarrow ++-+$ splitting. There are two $2 \rightarrow 3$ splittings that contribute to the $j \parallel k$ limit:

$$\begin{aligned} (++)+ &\rightarrow (+-)+, \\ +(++) &\rightarrow (+-+). \end{aligned}$$

Demanding that these two splittings give the correct collinear limit for $j \parallel k$ corresponding to a $+ \rightarrow +-$ gluon splitting demands that

$$h_1(z) + \frac{1}{1-z} + g(1-z) = \frac{z^3}{1-z}. \quad (29)$$

In addition to the collinear limit constraints we must also demand that the spin-dependent antennae sum to reproduce the spin-summed antennae as listed in tab. 6 as well as the positivity requirements. First, considering the spin-summed requirement, the numerators of the splitting functions must sum appropriately:

$$\begin{aligned} -2 - \alpha + (1 + 2\alpha)z - z^2 &= f(z) + h_1(z) + a_1(z) + c_1(z) \\ &= f(z) + h_2(z) + a_2(z) + c_2(z) \\ &= g(z) + h_2(z) + b_1(z) + c_2(z) \\ &= g(z) + h_1(z) + b_2(z) + c_1(z). \end{aligned} \quad (30)$$

α is the parameter of the spin-summed global antennae as defined in the previous appendix. The positivity requirements can be applied to each antenna function individually, and, in general, the two collinear limits can be used to constrain each antenna; namely $y_{ij} \rightarrow 0, y_{jk} > 0$ and $y_{jk} \rightarrow 0, y_{ij} > 0$. This leads to the following inequalities:

$$\begin{aligned} \frac{1}{z} + f(z) \geq 0, & \quad \frac{1}{z} + a_1(z) \geq 0, & \quad \frac{1}{z} + a_2(z) \geq 0, & \quad c_1(z) \geq 0, & \quad c_2(z) \geq 0 \\ \frac{1}{z} + g(z) \geq 0, & \quad \frac{1}{z} + b_1(z) \geq 0, & \quad \frac{1}{z} + b_2(z) \geq 0, & \quad h_1(z) \geq 0, & \quad h_2(z) \geq 0 \end{aligned} \quad (31)$$

where $0 < z \leq 1$ in the final-state shower phase space.

Imposing all constraints from eq. (28), eq. (30) and eq. (31), the singular terms in the helicity-dependent global antennae for gluon emission can be written as:

$$\begin{aligned}
++ \rightarrow +++ &= \frac{1}{y_{ij}y_{jk}} + \frac{(\alpha_1 - \alpha + 1) - 2(\alpha_1 - \alpha + 1)y_{jk}}{y_{ij}} + \frac{(\alpha_1 - \alpha + 1) - 2(\alpha_1 - \alpha + 1)y_{ij}}{y_{jk}} \\
++ \rightarrow +-+ &= \frac{1}{y_{ij}y_{jk}} + \frac{-(\alpha_1 + 3) + (2\alpha_1 + 3 - \beta_1)y_{jk} - (\alpha_1 + 1 - \beta_1)y_{jk}^2}{y_{ij}} \\
&\quad + \frac{-(\alpha_1 + 3) + (2\alpha_1 + 3 - \beta_1)y_{ij} - (\alpha_1 + 1 - \beta_1)y_{ij}^2}{y_{jk}} \\
++ \rightarrow -++ &= \frac{\beta_1 y_{jk} + (\alpha_1 - \beta_1)y_{jk}^2}{y_{ij}} \\
++ \rightarrow +++ &= \frac{\beta_1 y_{ij} + (\alpha_1 - \beta_1)y_{ij}^2}{y_{jk}} \\
+- \rightarrow +++ &= \frac{1}{y_{ij}y_{jk}} + \frac{(\alpha_1 - \alpha + 1) - 2(\alpha_1 - \alpha + 1)y_{jk}}{y_{ij}} \\
&\quad + \frac{-(\alpha_1 + 3) + (2\alpha_1 + 3 - \beta_1)y_{ij} - (\alpha_1 + 1 - \beta_1)y_{ij}^2}{y_{jk}} \\
+- \rightarrow +-+ &= \frac{1}{y_{ij}y_{jk}} + \frac{-(\alpha_1 + 3) + (2\alpha_1 + 3 - \beta_1)y_{jk} - (\alpha_1 + 1 - \beta_1)y_{jk}^2}{y_{ij}} \\
&\quad + \frac{(\alpha_1 - \alpha + 1) - 2(\alpha_1 - \alpha + 1)y_{ij}}{y_{jk}} \\
+- \rightarrow +-+ &= \frac{\beta_1 y_{ij} + (\alpha_1 - \beta_1)y_{ij}^2}{y_{jk}} \\
+- \rightarrow -+- &= \frac{\beta_1 y_{jk} + (\alpha_1 - \beta_1)y_{jk}^2}{y_{ij}}
\end{aligned}$$

for the parameters α , α_1 and β_1 . α is the spin-summed parameter which can be set appropriately to compare the spin-dependent antennae to the corresponding spin-summed or unpolarized antennae. The constraints on positivity are that $\alpha \geq 0$, $0 \leq \alpha_1 \leq \alpha$ and $\beta_1 \geq 0$.

We also must impose the constraint that all antennae are positive in the non-singular regions of phase space. This requires that finite terms are added to some spin-dependent antennae. The procedure for determining the non-singular terms will be discussed in appendix A.3 and similar non-singular terms are found in the global case as in the sector case. These non-singular terms are included in tab. 3.

A.3 Construction of Helicity-Dependent Sector Antennae

In this appendix, we will provide an example of how the sector antennae are constructed from their singular limits. Consider the splitting $g_+g_+ \rightarrow g_+g_-g_+$ to three final-state gluons i , j and k , respectively. The singular terms of the sector antenna for this splitting can be written in the generic form as

$$a(g_+g_+ \rightarrow g_+g_-g_+) = \frac{1}{y_{ij}y_{jk}} + \frac{f(y_{jk})}{y_{ij}} + \frac{f(y_{ij})}{y_{jk}}, \quad (32)$$

for some function $f(z)$. The form of this antenna is constrained by its soft and collinear limits. The eikonal term, $1/y_{ij}y_{jk}$, is required by the existence of a soft limit for the emission of the negative helicity gluon for this splitting. The other terms are constrained by the form of the collinear limits. Note that the splitting is symmetric under the interchange of gluons i and k which demands that the numerator of the terms proportional to $1/y_{ij}$ and $1/y_{jk}$ be identical. Thus, to determine the full form of the singular terms, we only need to consider a single collinear limit.

In the limit that $i \parallel j$, the antenna must reproduce the splitting function:

$$a(g_+g_+ \rightarrow g_+g_-g_+) \xrightarrow{i \parallel j} \frac{1}{y_{ij}} P_{g_-g_+\leftarrow g_+}(z) = \frac{1}{y_{ij}} \frac{(1-z)^3}{z}, \quad (33)$$

where z is the energy fraction of the emitted negative helicity gluon. In this limit, $y_{ij} \rightarrow 0$ and $y_{jk} \rightarrow z$ and this constrains the function $f(z)$:

$$a(g_+g_+ \rightarrow g_+g_-g_+) \xrightarrow{i \parallel j} \frac{1}{y_{ij}} \left(\frac{1}{z} + f(z) \right) = \frac{1}{y_{ij}} \frac{(1-z)^3}{z}. \quad (34)$$

It follows that $f(z) = -3 + 3z - z^2$ and thus the antenna is

$$\begin{aligned} a(g_+g_+ \rightarrow g_+g_-g_+) &= \frac{1}{y_{ij}y_{jk}} - \frac{3}{y_{ij}} - \frac{3}{y_{jk}} + 3\frac{y_{jk}}{y_{ij}} + 3\frac{y_{ij}}{y_{jk}} - \frac{y_{jk}^2}{y_{ij}} - \frac{y_{ij}^2}{y_{jk}} \\ &+ \text{non-singular terms} \end{aligned} \quad (35)$$

This form of the antenna produces the correct limiting behavior. However, to be able to use the antenna in a Markov chain Monte Carlo, it must also have the interpretation as a probability density and so must be non-negative on all of phase space. Currently, VINCIA only showers the final state, so we will only consider the final-state phase space for this antenna. Note that, for example, at the point $y_{ij} = y_{jk} = 1/2$, the singular terms of the antenna sum to the value -3 . Therefore, we must carefully add non-singular terms to the antenna to guarantee positivity.

To do this, we will find the minima of the antenna on final-state phase space and add the minimal non-singular terms necessary to guarantee positivity. By the symmetry of the antenna, the minima lies on the line $y_{ij} = y_{jk} = x$. Along this line, the derivative of the singular terms of the antenna is

$$\frac{d}{dx} a(g_+g_+ \rightarrow g_+g_-g_+)_{\text{sing}} = -\frac{2}{x^3} + \frac{6}{x^2} - 2. \quad (36)$$

Demanding that the derivative be zero at the minima produces a cubic equation with an irrational solution on phase space. To simplify this, we add the non-singular term $y_{ij} + y_{jk}$ to the original antenna. This term removes the -2 from the derivative producing a very simple equation to find the minima of the modified antenna. The minima is located at $x = 1/3$ where the modified antenna takes the value -3 . Therefore, the following antenna is used for the splitting $g_+g_+ \rightarrow g_+g_-g_+$ in the sector shower in VINCIA:

$$a(g_+g_+ \rightarrow g_+g_-g_+) = \frac{1}{y_{ij}y_{jk}} - \frac{3}{y_{ij}} - \frac{3}{y_{jk}} + 3\frac{y_{jk}}{y_{ij}} + 3\frac{y_{ij}}{y_{jk}} - \frac{y_{jk}^2}{y_{ij}} - \frac{y_{ij}^2}{y_{jk}} + 3 + y_{ij} + y_{jk}. \quad (37)$$

This is non-negative on all of final-state phase space.

B Jeppsson 5 Tune Parameters

Note: the Jeppsson 5 parameter set is optimized for use with VINCIA and to some extent depends on the behavior of that shower model near the hadronization cutoff. It is therefore not advised to use this parameter set directly for standalone PYTHIA 8.

```
! * alphaS
Vincia:alphaSvalue      = 0.139  ! alphaS(mZ) value
Vincia:alphaSkMu        = 1.0    ! Renormalization-scale prefactor
Vincia:alphaSorder      = 1      ! Running order
Vincia:alphaSmode       = 1      ! muR = pT:emit and Q:split
Vincia:alphaScmw        = off     ! CMW rescaling of Lambda on/off

! * Shower evolution and IR cutoff
Vincia:evolutionType    = 1      ! pT-evolution
Vincia:orderingMode     = 2      ! Smooth ordering
Vincia:pTnormalization  = 4.     ! QT = 2pT
Vincia:cutoffType       = 1      ! Cutoff taken in pT
Vincia:cutoffScale      = 0.6    ! Cutoff value (in GeV)

! * Longitudinal string fragmentation parameters
StringZ:aLund           = 0.38   ! Lund FF a (hard fragmentation supp)
StringZ:bLund           = 0.90   ! Lund FF b (soft fragmentation supp)
StringZ:aExtraDiquark   = 1.0    ! Extra a to suppress hard baryons

! * pT in string breakups
StringPT:sigma          = 0.275  ! Soft pT in string breaks (in GeV)
StringPT:enhancedFraction = 0.01  ! Fraction of breakups with enhanced pT
StringPT:enhancedWidth  = 2.0    ! Enhancement factor

! * String breakup flavor parameters
StringFlav:probStoUD    = 0.215  ! Strangeness-to-UD ratio
StringFlav:mesonUDvector = 0.45   ! Light-flavor vector suppression
StringFlav:mesonSvector = 0.65   ! Strange vector suppression
StringFlav:mesonCvector = 0.80   ! Charm vector suppression
StringFlav:probQQtOQ    = 0.083  ! Diquark rate (for baryon production)
StringFlav:probSQtoQQ   = 1.00   ! Optional Strange diquark suppression
StringFlav:probQQ1toQQ0 = 0.031  ! Vector diquark suppression
StringFlav:etaSup       = 0.68   ! Eta suppression
StringFlav:etaPrimeSup  = 0.11   ! Eta' suppression
StringFlav:decupletSup  = 1.0    ! Optional Spin-3/2 Baryon Suppression
```

References

- [1] A. Buckley, J. Butterworth, S. Gieseke, D. Grellscheid, S. Hoche, *et al.*, “General-purpose event generators for LHC physics,” *Phys.Rept.* **504** (2011) 145–233, [1101.2599](#).
- [2] S. Catani, F. Krauss, R. Kuhn, and B. Webber, “QCD matrix elements + parton showers,” *JHEP* **0111** (2001) 063, [hep-ph/0109231](#).

- [3] L. Lönnblad, “Correcting the color dipole cascade model with fixed order matrix elements,” *JHEP* **0205** (2002) 046, [hep-ph/0112284](#).
- [4] M. L. Mangano, M. Moretti, F. Piccinini, and M. Treccani, “Matching matrix elements and shower evolution for top-pair production in hadronic collisions,” *JHEP* **01** (2007) 013, [hep-ph/0611129](#).
- [5] K. Hamilton and P. Nason, “Improving NLO-parton shower matched simulations with higher order matrix elements,” *JHEP* **1006** (2010) 039, [1004.1764](#).
- [6] P. Skands, “Introduction to QCD,” [1207.2389](#).
- [7] J. J. Lopez-Villarejo and P. Skands, “Efficient Matrix-Element Matching with Sector Showers,” *JHEP* **1111** (2011) 150, [1109.3608](#).
- [8] M. Bengtsson and T. Sjöstrand, “Coherent Parton Showers Versus Matrix Elements: Implications of PETRA - PEP Data,” *Phys.Lett.* **B185** (1987) 435.
- [9] W. Giele, D. Kosower, and P. Skands, “Higher-Order Corrections to Timelike Jets,” *Phys.Rev.* **D84** (2011) 054003, [1102.2126](#).
- [10] A. J. Larkoski and M. E. Peskin, “Spin-Dependent Antenna Splitting Functions,” *Phys.Rev.* **D81** (2010) 054010, [0908.2450](#).
- [11] P. Richardson, “Spin correlations in Monte Carlo simulations,” *JHEP* **0111** (2001) 029, [hep-ph/0110108](#).
- [12] R. K. Ellis, W. J. Stirling, and B. R. Webber, *QCD and Collider Physics*. Cambridge University Press, 1996.
- [13] W. T. Giele, D. A. Kosower, and P. Z. Skands, “A Simple shower and matching algorithm,” *Phys.Rev.* **D78** (2008) 014026, [0707.3652](#).
- [14] S. J. Parke and T. Taylor, “An Amplitude for n Gluon Scattering,” *Phys.Rev.Lett.* **56** (1986) 2459.
- [15] G. Altarelli and G. Parisi, “Asymptotic Freedom in Parton Language,” *Nucl.Phys.* **B126** (1977) 298.
- [16] E. Boos, M. Dobbs, W. Giele, I. Hinchliffe, J. Huston, *et al.*, “Generic user process interface for event generators,” [hep-ph/0109068](#).
- [17] A. Gehrmann-De Ridder, T. Gehrmann, and E. N. Glover, “Antenna subtraction at NNLO,” *JHEP* **0509** (2005) 056, [hep-ph/0505111](#).
- [18] J. Alwall, P. Demin, S. de Visscher, R. Frederix, M. Herquet, *et al.*, “MadGraph/MadEvent v4: The New Web Generation,” *JHEP* **0709** (2007) 028, [0706.2334](#).
- [19] H. Murayama, I. Watanabe, and K. Hagiwara, “HELAS: HELicity amplitude subroutines for Feynman diagram evaluations,”.
- [20] A. Gehrmann-De Ridder, M. Ritzmann, and P. Skands, “Timelike Dipole-Antenna Showers with Massive Fermions,” *Phys.Rev.* **D85** (2012) 014013, [1108.6172](#).

- [21] A. J. Larkoski and M. E. Peskin, “Antenna Splitting Functions for Massive Particles,” *Phys.Rev.* **D84** (2011) 034034, [1106.2182](#).
- [22] P. Z. Skands and S. Weinzierl, “Some remarks on dipole showers and the DGLAP equation,” *Phys.Rev.* **D79** (2009) 074021, [0903.2150](#).
- [23] R. Kleiss, W. J. Stirling, and S. Ellis, “A new Monte Carlo treatment multiparticle phase space at high energies,” *Comput.Phys.Commun.* **40** (1986) 359.
- [24] L. Lönnblad and S. Prestel, “Unitarising Matrix Element + Parton Shower merging,” [1211.4827](#).
- [25] P. D. Draggotis, A. van Hameren, and R. Kleiss, “SARGE: An Algorithm for generating QCD antennas,” *Phys.Lett.* **B483** (2000) 124–130, [hep-ph/0004047](#).
- [26] W. T. Giele, G. C. Stavenga, and J.-C. Winter, “A Forward Branching Phase-Space Generator,” [1106.5045](#).
- [27] T. Gleisberg, S. Hoeche, F. Krauss, M. Schonherr, S. Schumann, *et al.*, “Event generation with SHERPA 1.1,” *JHEP* **0902** (2009) 007, [0811.4622](#).
- [28] B. Andersson, “The Lund model,” *Camb.Monogr.Part.Phys.Nucl.Phys.Cosmol.* **7** (1997) 1–471.
- [29] T. Gleisberg and S. Hoeche, “Comix, a new matrix element generator,” *JHEP* **0812** (2008) 039, [0808.3674](#).
- [30] I. Antcheva, M. Ballintijn, B. Bellenot, M. Biskup, R. Brun, *et al.*, “ROOT: A C++ framework for petabyte data storage, statistical analysis and visualization,” *Comput.Phys.Commun.* **180** (2009) 2499–2512.
- [31] **L3 Collaboration** Collaboration, P. Achard *et al.*, “Studies of hadronic event structure in e^+e^- annihilation from 30-GeV to 209-GeV with the L3 detector,” *Phys.Rept.* **399** (2004) 71–174, [hep-ex/0406049](#).
- [32] A. Buckley, H. Hoeth, H. Lacker, H. Schulz, and J. E. von Seggern, “Systematic event generator tuning for the LHC,” *Eur.Phys.J.* **C65** (2010) 331–357, [0907.2973](#).
- [33] P. Z. Skands, “Tuning Monte Carlo Generators: The Perugia Tunes,” *Phys.Rev.* **D82** (2010) 074018, [1005.3457](#).
- [34] R. Corke and T. Sjöstrand, “Interleaved Parton Showers and Tuning Prospects,” *JHEP* **1103** (2011) 032, [1011.1759](#).
- [35] S. Catani, B. Webber, and G. Marchesini, “QCD coherent branching and semiinclusive processes at large x ,” *Nucl.Phys.* **B349** (1991) 635–654.
- [36] L. Hartgring, E. Laenen, and P. Skands, “Antenna showers with one-loop matrix elements,” (2013). in preparation.
- [37] **ALEPH Collaboration** Collaboration, A. Heister *et al.*, “Studies of QCD at e^+e^- centre-of-mass energies between 91-GeV and 209-GeV,” *Eur.Phys.J.* **C35** (2004) 457–486.

- [38] **DELPHI Collaboration** Collaboration, J. Abdallah *et al.*, “Determination of the b quark mass at the M(Z) scale with the DELPHI detector at LEP,” *Eur.Phys.J.* **C46** (2006) 569–583, [hep-ex/0603046](#).
- [39] S. Catani, Y. L. Dokshitzer, M. Olsson, G. Turnock, and B. Webber, “New clustering algorithm for multi - jet cross-sections in e+ e- annihilation,” *Phys.Lett.* **B269** (1991) 432–438.
- [40] M. Cacciari, G. P. Salam, and G. Soyez, “FastJet User Manual,” *Eur.Phys.J.* **C72** (2012) 1896, [1111.6097](#).
- [41] **Particle Data Group** Collaboration, J. Beringer *et al.*, “Review of Particle Physics (RPP),” *Phys.Rev.* **D86** (2012) 010001.
- [42] A. Buckley and M. Whalley, “HepData reloaded: Reinventing the HEP data archive,” *PoS ACAT2010* (2010) 067, [1006.0517](#).
- [43] M. Ritzmann, D. Kosower, and P. Skands, “Antenna Showers with Hadronic Initial States,” [1210.6345](#).
- [44] F. A. Berends and W. Giele, “Recursive Calculations for Processes with n Gluons,” *Nucl.Phys.* **B306** (1988) 759.
- [45] F. Krauss, R. Kuhn, and G. Soff, “AMEGIC++ 1.0: A Matrix element generator in C++,” *JHEP* **0202** (2002) 044, [hep-ph/0109036](#).
- [46] C. Berger, Z. Bern, L. Dixon, F. Febres Cordero, D. Forde, *et al.*, “An Automated Implementation of On-Shell Methods for One-Loop Amplitudes,” *Phys.Rev.* **D78** (2008) 036003, [0803.4180](#).
- [47] S. Badger, B. Biedermann, L. Hackl, J. Plefka, T. Schuster, *et al.*, “Comparing efficient computation methods for massless QCD tree amplitudes: Closed Analytic Formulae versus Berends-Giele Recursion,” [1206.2381](#).
- [48] G. Gustafson and U. Pettersson, “Dipole Formulation of QCD Cascades,” *Nucl.Phys.* **B306** (1988) 746.
- [49] L. Lönnblad, “ARIADNE version 4: A Program for simulation of QCD cascades implementing the color dipole model,” *Comput.Phys.Commun.* **71** (1992) 15–31.